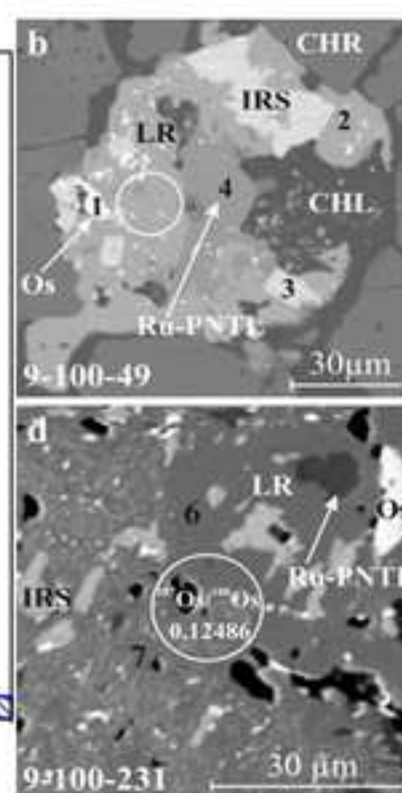
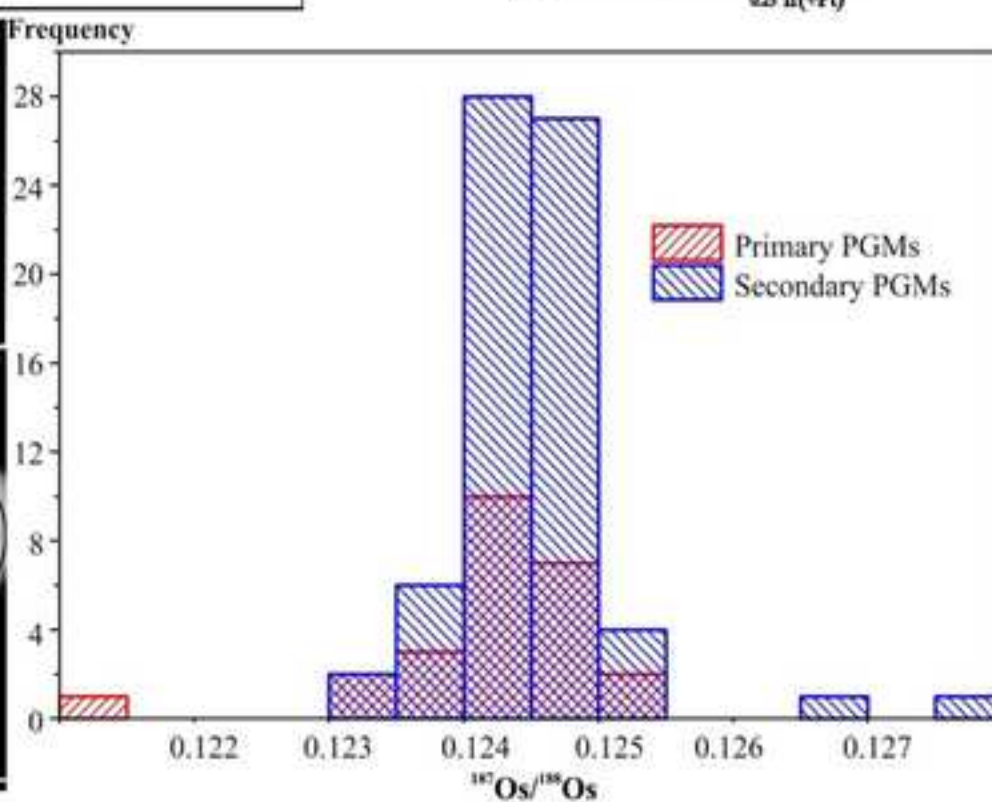
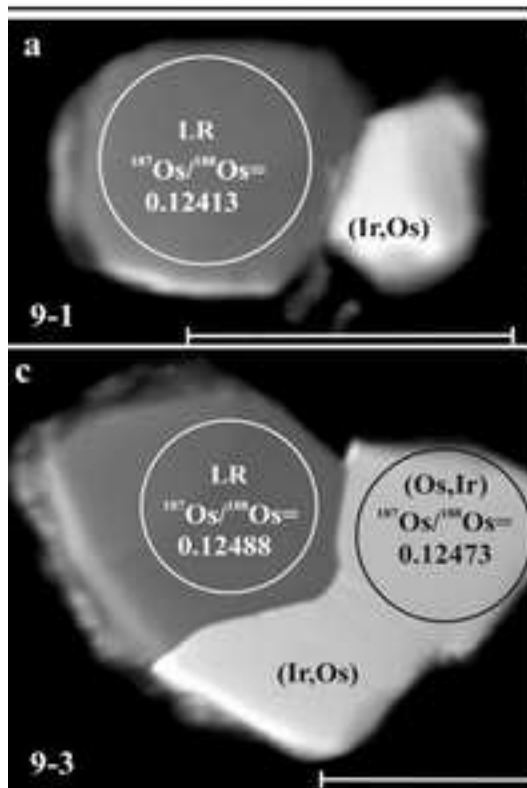
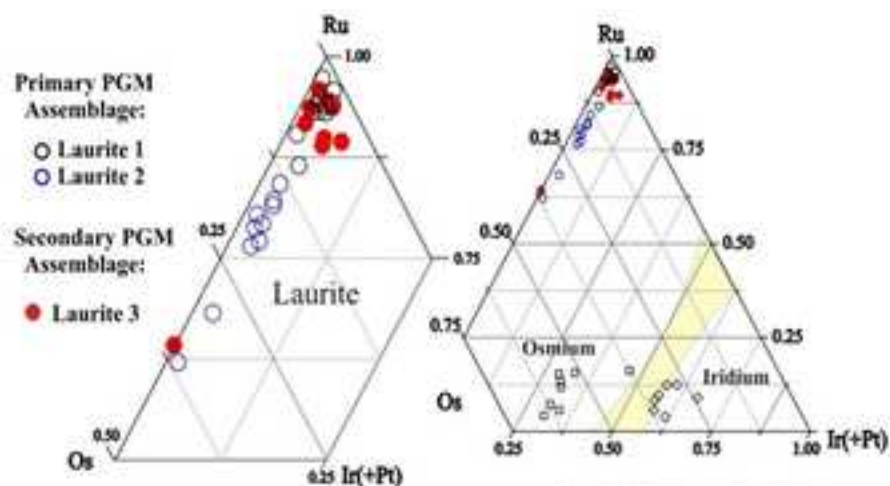
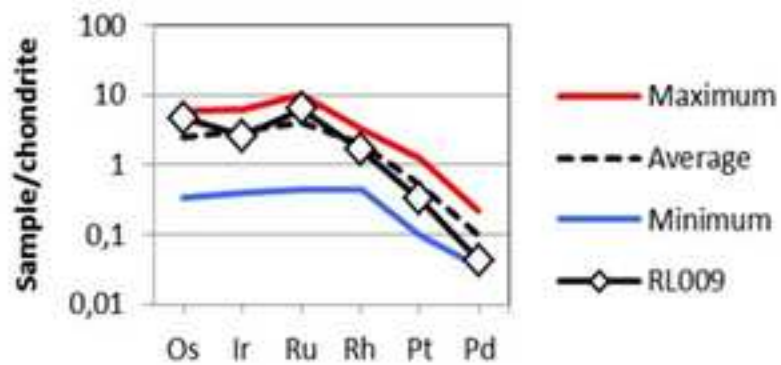


Harold's Grave chromitites



Highlights

- ▶ Two distinct PGM assemblages in a mantle chromitite of the Shetland Ophiolite Complex.
- ▶ Primary and secondary PGM assemblages have similarly unradiogenic $^{187}\text{Os}/^{188}\text{Os}$ values.
- ▶ Whole-rock Os isotope budget is controlled by the laurite-dominant PGM assemblages.
- ▶ Mantle Os-isotope signature is preserved during crustal alteration processes.
- ▶ Os-isotope data support an Enstatite Chondrite Reservoir model for the upper mantle.

31 0.12488) and similar ‘unradiogenic’ $^{187}\text{Os}/^{188}\text{Os}$ values for both ‘primary’ and ‘secondary’ PGM assemblages
32 (0.1242±0.0008 and 0.1245±0.0006, respectively), which closely match the bulk $^{187}\text{Os}/^{188}\text{Os}$ value of their host
33 chromitite (0.1240±0.0006). The unprecedented isotopic similarity between primary or secondary PGM
34 assemblages and chromitite we report suggests that the osmium isotope budget of chromitite is largely controlled
35 by the contained laurite and Os-rich alloy. This demonstrates that closed system behaviour of the Re-Os isotope
36 system is possible, even during complex postmagmatic hydrothermal and/or metamorphic events. The preserved
37 mantle Os-isotope signatures provide further support for an Enstatite Chondrite Reservoir (ECR) model for the
38 convective upper mantle and are consistent with origin of the complex as a Caledonian ophiolite formed in a
39 supra-subduction zone setting shortly before obduction.

40 *Keywords:* platinum-group minerals, chromitite, osmium isotopes, mantle, Harold’s Grave, Shetland
41 Ophiolite Complex

42 43 **Introduction**

44
45 Osmium isotopes are considered as important tracers for understanding the evolution of highly siderophile
46 elements (HSE) in the upper mantle. Due to the progress of analytical techniques in recent years, the Re-Os
47 system has been widely applied for evaluating distinct mantle sources and dating melting events in the mantle in
48 different geological settings (see Shirey and Walker, 1998; Carlson, 2005; Rudnick and Walker, 2009 and
49 references therein). In contrast to the geochemical properties of strontium, neodymium, hafnium, and lead, all of
50 which are incompatible elements, osmium behaves as compatible element during mantle melting processes
51 leading to high Os contents in the residual mantle (Barnes et al., 1985; Hart and Ravizza, 1996; Burton et al.,
52 1999; 2002, among others).

53 Although considered more robust than lithophile element based isotopic systems, it was suggested that
54 the Re-Os isotopic system is not entirely immune to resetting and disruptions (Brandon et al., 1996; Becker et
55 al., 2001, Le Roux et al., 2009; O’Reilly and Griffin, 2012 and references therein). Ambiguity in the use and
56 interpretation of whole rock Os isotope data also arose from a number of mineral-scale Os-isotopic studies
57 (Burton et al., 1999; Alard et al., 2002; 2005, etc.), which proved the existence of inter-mineral ‘Os-
58 heterogeneity’ within individual samples. These studies showed that the unradiogenic Os isotopic signature of
59 base-metal sulfides enclosed in silicate can easily be masked by external highly radiogenic secondary BM
60 sulfides and thus cannot be estimated from whole rock Os isotopes alone. This necessitates careful evaluation of
61 different mineral phases to evaluate the significance of the whole rock Re-Os isotope signatures and model ages
62 (Reisberg et al., 2004). The Os isotopic system of minerals such as chromite, olivine, base-metal sulfide, Ru-Os

63 sulfide and Os-rich alloy may contribute to a better understanding and more accurate interpretation of the
64 processes that govern the behaviour of Os isotopes in different mantle environments (Hattori and Hart, 1991;
65 Burton et al., 1999; Standish et al., 2001; Alard et al., 2002; 2005; Walker et al., 2002b; Malitch et al., 2003a;
66 Ahmed et al., 2006; Brandon et al., 2006; Pearson et al., 2007; Shi et al., 2007; Nowell et al., 2008; Marchesi et
67 al., 2011; Badanina et al., 2014; González-Jiménez et al., 2014; Luguét et al., 2015). Primary Os-bearing PGM
68 (laurite-erlichmanite series, RuS₂-OsS₂ and Ru-Os-Ir alloys) that form inclusions in chromite are particularly
69 important because these are well protected by the host mineral and presumably preserve initial Os isotope values
70 of the source the Ru-Os sulfides and Ru-Os-Ir alloys were crystallized. The Os budget of the mantle is mainly
71 controlled by sulfides and alloys (Martin et al., 1993; Hart and Ravizza, 1996; Burton et al., 1999) so combining
72 micro-analysis of both Os-bearing sulfides and alloys, coupled with whole rock data, offers a way to test for
73 intra-sample heterogeneity and hence allows a more robust interpretation of the Os-isotope systematics.

74 Two contrasting types of PGM suite are known to occur in podiform chromitites from within the mantle
75 sequence of the Shetland Ophiolite Complex (SOC). These include both IPGE- (i.e., Os, Ir, Ru) and PPGE- (Rh,
76 Pt, Pd) rich assemblages, which are exemplified by two type localities, referred to by the nearby place names of
77 Harold's Grave and Cliff, respectively (Prichard et al., 1986; Tarkian and Prichard, 1987; Prichard and Tarkian,
78 1988). These studies used the textural position of PGMs with respect to the silicate host to suggest that Os- and
79 Ru-rich PGM formed before those of Ir-, Pd-, Rh- and, lastly, Pt-bearing PGM. Only Os-rich laurite occurred
80 enclosed by unaltered chromite, with other PGMs either in the altered rim of chromite grains or in interstitial
81 altered silicates, with sperrylite (PtAs₂) found exclusively in the latter textural position. Two distinct platinum-
82 group mineral (PGM) assemblages have been recognized at Harold's Grave (Badanina et al., 2013a): a 'primary'
83 euhedral PGM assemblage, which occurs as inclusions in chromite, and a modified 'secondary' subhedral to
84 anhedral PGM assemblage observed in cracks filled by chlorite or serpentine, interstitially to chromite grains.
85 The 'primary' PGM assemblage is represented by solitary grains of laurite or Os-rich iridium and composite
86 grains of laurite + Os-rich iridium ± Ir-rich osmium, whereas the 'secondary' PGM assemblage is defined by
87 laurite, Os-rich laurite, irarsite, native osmium and Ru-pentlandite.

88 Our current study is directed towards identifying the Os-isotope composition of both primary and
89 secondary laurite-alloy assemblages as revealed in individual composite grains enclosed within or interstitially to
90 chromite, respectively, since these are rarely reported from ophiolite deposits (Malitch et al., 2003a; 2014; 2016;
91 González-Jiménez et al., 2012b; 2015). We present in-situ Os-isotope compositions of primary and secondary
92 PGM assemblages from Harold's Grave, along with their PGM chemistry and the whole rock PGE and Os-
93 isotope composition of the host chromitite in order to: 1) compare the isotope signatures of the chromitite,

94 primary and secondary PGM assemblages, and 2) constrain the long-term Re-Os evolution of the Earth's upper
95 mantle as exemplified by this Late Paleozoic ophiolite complex.

96

97 **Geological background and sample location**

98

99 The Shetland islands of Unst and Fetlar, lie roughly midway between Norway and the Scottish mainland. The
100 ultramafic and mafic complex outcropping here was first described as an ophiolite complex by Garson and Plant
101 (1973), an interpretation supported by the majority of subsequent authors (e.g. Flinn et al., 1979, Flinn, 1985;
102 Prichard, 1985). At least two stacked nappes of ophiolitic lithologies are recognized in the Shetland Ophiolite
103 Complex, representing an original structural thickness of 8-10 km (Fig.1, Flinn, 1985; 2001 and references
104 therein). The variably serpentinised protoliths and characteristic stratigraphic of tectonised harzburgite, cumulate
105 dunite, werhlite-pyroxenite layers and isotropic gabbros are recognizable, together with intercalated fragments of
106 a dynamo-metamorphic sole and lower grade metasedimentary rocks (Prichard, 1985). Irregular and isolated
107 podiform chromitite layers, up to 2 m thick, occur in dunite pods or cumulates (Prichard and Lord, 1993).

108 Crystallization of the SOC is constrained to before 492 ± 3 Ma by the U-Pb age of zircon from a
109 plagiogranite (Spray and Dunning, 1991), with intra-oceanic thrusting, obduction and/or subsequent thrusting
110 constrained to between 479 ± 6 Ma and 465 ± 5 Ma by K-Ar data from hornblende in the metamorphic sole
111 (Spray, 1988). A boninitic dyke swarm cutting gabbros at the uppermost exposed stratigraphic level of the
112 complex indicates a supra-subduction zone setting (Prichard and Lord, 1988), which may provide an explanation
113 for the unusually high concentrations of PGE for an ophiolite complex, in particularly for PPGE (Prichard et al.,
114 1996). These are found associated with chromite and weakly disseminated sulfides, located either in dunite pods
115 in harzburgite, or in stratiform discontinuous chromite-rich dunites within the lower crustal sequence above the
116 petrological moho, or with minor sulfide concentrations in pyroxene-rich rocks above, exemplified by the area
117 North of Baltasound (Prichard et al., 1986; Lord, 1991; Lord et al., 1994; Lord and Prichard, 1997; O'Driscoll et
118 al., 2012; Brough et al., 2015). Highly PPGE-enriched chromite-rich lithologies at Cliff have been attributed to
119 subsequent hydrothermal mineralisation during talc-carbonate alteration (Gunn and Styles, 2002) or to localized
120 in situ upgrading of existing magmatic concentrations (Lord et al., 1994). The mineralogy of the Os-, Ir-, Ru-
121 and Rh-bearing PGM from these chromitites and other lithologies have been evaluated elsewhere (Tarkian and
122 Prichard 1987; Prichard and Tarkian, 1988; Prichard et al., 1986; 1994) including those from Harold's Grave
123 (Prichard et al., 1986; Tarkian and Prichard, 1987; Prichard and Tarkian, 1988; Badanina et al., 2013a). The
124 compositionally heterogenous character of chromitite occurrences and their late-stage alteration has been
125 reported by Derbyshire et al. (2013) and Brough et al. (2015).

126 The Harold's Grave locality lies 0.75 km N of the east-west trending petrological Moho and the main
127 concentration of chromite quarries. Although poorly exposed, protolith mapping has shown it is associated with
128 an exceptionally large dunite pod ca. 500 m long (Fig. 2, Lord, 1991), which has been interpreted as evidence of
129 a larger throughput of magma from which to source IPGE (Brough et al., 2015). The textures of the chromite-
130 rich lithologies are particularly massive (Fig. 3), which may be interlayered with serpentinized dunite. The area
131 is one of the least affected by talc-carbonate alteration of any chromite-rich mantle pod and sufficiently remote
132 to discount any possibility of ore material being transported from other locations, so was selected as ideal for
133 detailed investigation of primary Os isotopes. The material investigated here was from a sub-sample of a single
134 boulder of stockpiled chromitite associated with the trial excavation and was exceptionally large (ca. 10 kg)
135 compared to the ore grade material remaining in the other worked-out locations in the SOC.

136

137 **Analytical techniques**

138

139 The study combined a number of analytical techniques, including acid digestion and isotope dilution (ID) ICP-
140 MS, electron microprobe analysis and laser-ablation attached to multiple collector inductively coupled plasma
141 mass spectrometry (LA MC-ICP-MS). Whole-rock PGE- and Re-concentrations, and the Os-isotope composition
142 were determined through the application of the high pressure asher acid digestion and ID-ICP-MS method
143 detailed by Meisel et al. (2001a; 2003) and Paliulionyte et al. (2006). In brief, a test portion of 2 g of fine grained
144 chromitite sample powder was spiked with a mixed PGE and Re solution, digested in an acid mixture (5 ml of
145 concentrated HNO₃ and 2 ml of concentrated HCl) at 300 °C and 125 bar (1.25*10⁷ Pa) for 10 hours in a high
146 pressure asher (HPA-S, Anton Paar, Graz, Austria). The osmium concentration was determined by sparging the
147 OsO₄ that was formed during digestion into the ICP-QMS 7500ce at the General and Analytical Chemistry,
148 Montanuniversität Leoben. The ¹⁸⁷Os/¹⁸⁸Os value was calculated after spike and internal mass bias correction.
149 The absolute amount of the analysed inhouse Os reference solution LOsST was equal to two ng of Os. Repeated
150 measurement of the standard solution over a period of two years gave ¹⁸⁷Os/¹⁸⁸Os=0.1069 with a standard
151 deviation of less than 1%. The remaining solution was dried down and the Ru, Pd, Re, Ir and Pt concentrations
152 were determined with an on-line separation procedure as outlined by Meisel et al. (2003). Blanks for Re and Os
153 were always less than 10 pg.

154 The textural relationships of PGM with the associated gangue minerals were investigated in polished
155 sections using an ARL-SEMQ microprobe equipped with four wavelength-dispersive spectrometers (WDS) and
156 a LINK energy dispersive analyser at the Chair of Resource Mineralogy, Montanuniversität Leoben (Austria).
157 About 2.5 kg of the chromitite sample was disintegrated and milled, followed by sieving and removal of the fine

158 fractions <56 and 56–100 microns. The heavy minerals (including PGMs) within these two fractions were
159 concentrated by a hydroseparation technique (Knauf, 1996; Malitch et al., 2001; Rudashevsky et al., 2002) at
160 NATI Research JSC, St. Petersburg, Russia (<http://www.natires.com>). Each heavy-mineral concentrate was
161 mounted in epoxy blocks and polished in separate sections for further detailed mineralogical and microanalytical
162 studies. About 1060 platinum-group mineral grains have been examined. Microprobe analyses of PGMs were
163 carried out with an ARL-SEM-Q microprobe with four WDS and equipped with a LINK energy dispersive
164 analyser (Montanuniversität Leoben) and a CAMECA SX-100 equipped with five WDS spectrometers and a
165 Bruker energy dispersive spectrometer system (Institute of Geology and Geochemistry, UB RAS). Details of the
166 analytical procedures are described by Malitch et al. (2001) and Badanina et al. (2013b).

167 The main set of LA measurements was performed with a Microprobe II LA device (Thermo Elemental,
168 Nd:YAG laser, 266 nm wavelength) and an AXIOM MC-ICPMS (Thermo Elemental Axiom, multicollector
169 version featuring 9 Faraday cup detectors operated at a mass resolution of 400) at the Technical University of
170 Mining and Metallurgy, Freiberg, Germany. The ICP-MS was tuned using a desolvating nebulizer (MCN 6000,
171 CETAC), a solution of 33 µg/l Re, 330 µg/l Os, and 330 µg/l Ir in 2% nitric acid, a nebulizer flow of 0.8 l/min
172 Ar, and a radio frequency (RF) forward power of 1330 W. Helium was used as an ablation chamber gas with a
173 flow of 85 ml/min that has minimised dead volume. The air capacitor of the ICP-MS was optimised to obtain a
174 RF reflected power of 12 to 18 W with this He addition to the plasma gas. The MC set-up, and corrections for Re
175 and W contents, were checked with combined laser ablation analyses of members of the hubnerite (MnWO₄) –
176 ferberite (FeWO₄) series and the aerosol generated by the desolvating nebulizer, as described by Junk (2001).
177 LA spots of 15 to 30 µm were used with a scan field that was adapted to the size of each sampling area (Figs. 4
178 and 5), a laser shot frequency of 20 Hz, and an energy output of up to 0.5 mJ. The aerosols generated by LA
179 were transported by a gas stream to the MC-ICP-MS. Nine signals were measured simultaneously at m/z 183
180 (W), 184 (W + Os), 185 (Re), 186 (W + Os), 187 (Re + Os), 188 (Os), 189 (Os), 191 (Ir) and 193 (Ir) using the
181 multichannel collector of the ICP-MS. The mass bias was corrected using an exponential fractionation law and
182 the ¹⁸⁸Os/¹⁸⁹Os ratio. All the analyzed grains have ¹⁸⁷Re/¹⁸⁸Os lower than 0.005, thus ensuring that the isobaric
183 interference of ¹⁸⁷Re on ¹⁸⁷Os was precisely corrected (cf. Nowell et al., 2008). The abundances used for the
184 calculations were taken from Rosman and Taylor (1998) (at.%, ¹⁸⁴Os = 0.02, ¹⁸⁶Os = 1.59, ¹⁸⁸Os = 13.24, ¹⁸⁹Os =
185 16.15, ¹⁹⁰Os = 26.26 and ¹⁹²Os = 40.78). The isotope ratios are reported with experimental uncertainties taking
186 into account the contributions of the Faraday cup efficiencies, the normalization value for mass bias corrections
187 using ¹⁸⁸Os/¹⁸⁹Os (Rosman and Taylor, 1998), interference corrections, the signal noise, and the within-run
188 standard deviations. Repeated analyses (n=36) of a natural Os–Ir alloy, which has been used to check the validity
189 of the LA MC-ICP-MS measurements, yield ¹⁸⁷Os/¹⁸⁸Os = 0.12166±0.00018 (2 sigma uncertainty). Furthermore,

190 it has been shown (Malitch et al., 2002) that the Os isotopic composition of Os–Ir alloy (i.e., Os_{0.89}Ir_{0.11}) from the
191 Bor-Uryah massif measured by LA MC-ICP-MS ($^{187}\text{Os}/^{188}\text{Os} = 0.12396 \pm 0.00013$) is in accordance with N-
192 TIMS analysis of the same sample ($^{187}\text{Os}/^{188}\text{Os} = 0.1240 \pm 0.0002$). A more detailed description of the LA MC-
193 ICP-MS technique is given by Junk (2001). In addition, 11 in-situ Os isotope analyses were carried out at
194 Geochemical Analysis Unit at the GEMOC laboratories (Macquarie University, Sydney, Australia, ESM
195 Appendix 1) using analytical methods described in detail by Pearson et al (2002), Marchesi et al. (2011) and
196 Gonzalez-Jimenez et al. (2015). These analyses used a Nu Plasma Multicollector ICP-MS attached to a New
197 Wave/Merchantek UP 213 laser microprobe. Ablation was carried out with a frequency of 4 Hz, energies of 1–2
198 mJ/pulse and a spot size ranging from 15 to 30 μm . A standard NiS bead (PGE-A) with 199 ppm Os (Lorand and
199 Alard, 2001) and $^{187}\text{Os}/^{188}\text{Os} = 0.1064$ (Pearson et al., 2002) was analyzed between PGM samples to monitor any
200 drift in the Faraday cups. These variations were typically less than 0.2% over an analytical session. The data
201 were collected using the Nu Plasma time-resolved software, which allows the selection of the most stable
202 intervals of the signal for integration. The selected interval was divided into 40 replicates to provide a measure of
203 the standard error. Under the ablation conditions described above, given the analyzed grains had average sizes >
204 100 μm and Os average contents of ~5 wt.%, a typical run duration of ~100 s was achieved with an average
205 signal intensity of Os ~1.9V on the Faraday cups. This gives a precision for $^{187}\text{Os}/^{188}\text{Os}$ ranging from 4.0×10^{-5} to
206 10.0×10^{-5} (SE). The accuracy of the data presented here is similar to that of Os–Ir alloys from chromitites in the
207 Luobusa (Tibet) Ophiolite as illustrated by independent data sets (different instruments, operating protocols); Shi
208 et al. (2007) reported a mean $^{187}\text{Os}/^{188}\text{Os} = 0.12646 \pm 11$ (1SE, n=148) while Pearson et al. (2007) reported
209 $^{187}\text{Os}/^{188}\text{Os} = 0.12653 \pm 7$ (1SE, n=80). The quoted uncertainties on T_{MA} and T_{RD} model ages include the
210 uncertainties in the measured $^{187}\text{Os}/^{188}\text{Os}$ and $^{187}\text{Re}/^{188}\text{Os}$, calculated according to the equation of Sambridge and
211 Lambert (1997).

212

213 **Results**

214

215 PGE concentrations and Os-isotope data in chromitite

216

217 The total PGE concentrations in the chromitite sample studied are typical of those reported for Harold's Grave
218 (Table 1) and at ΣPGE of 8587 ppb are very high compared to typical ophiolitic chromitite, for which total PGE
219 is commonly <500 ppb (Melcher, 2000). Consistently high whole-rock PGE concentrations in chromitites from
220 Harold's Grave give negatively sloped chondrite-normalized PGE patterns, typical of many mantle hosted
221 'ophiolitic' chromitites (Fig. 6), in which IPGE prevail over PPGE. The $^{187}\text{Os}/^{188}\text{Os}$ value of the chromitite at

222 Harold's Grave in this study (0.1240 ± 0.0006) is slightly less radiogenic than that of chromitite samples from the
223 same locality ($0.12489-0.12554$) presented by Walker et al. (2002b) and O'Driscoll et al. (2012).

224

225 Primary and secondary PGM assemblages at Harold's Grave

226

227 Following an extensive survey of 1060 PGM grains, two contrasting PGM assemblages have been shown to
228 occur at Harold's Grave, even within the same chromitite block (Table 2). These are distinguished by their
229 differing morphology and internal texture (Figure 4 and 5). Firstly, euhedral PGM up to (up to 55 μm in size)
230 occur as inclusions within chromite, indicating this is a "primary" magmatic assemblage; secondly, subeuhedral
231 to anhedral PGM (up to 500 μm) occur in association with pentlandite in serpentine- or chlorite-filled cracks or
232 interstitially to chromite grains, indicating a "secondary" modified assemblage. The primary PGM assemblage is
233 represented by 156 solitary grains of laurite and/or Os-rich iridium, or by polyphase groups of grains that display
234 regular phase boundaries between two or three distinct PGMs (Table 2, Fig. 4). The latter are predominately
235 laurite \pm Os-rich iridium (Fig. 4a, d), with subordinate examples of laurite + Os-rich iridium + Ir-rich osmium
236 (Fig. 4c) and more rarely laurite + Ir-Rh alloy + Rh-rich sulfide, possibly prassoite (Fig. 4b). In contrast, the
237 'secondary' PGM assemblage is represented by 904 grains, which are polyphase, complex and irregular. Again
238 laurite is dominant, but now intimately intergrown with Os-bearing laurite, native osmium, irarsite and Ru-rich
239 pentlandite (Table 2, Fig. 5). Other secondary PGM examples include the irarsite-hollingworthite series (IrAsS-
240 RhAsS), tolovkite (IrSbS), geversite (PtSb_2) and Ru-rich oxide, which occur in subordinate amounts (Table 2).

241 Table 3 gives representative analyses of PGMs that constitute secondary polyphase grains in Fig. 5,
242 whereas Fig. 7 shows the chemical variation of laurite and Os-rich alloys encountered. More detailed
243 compositional characteristics of the primary PGM assemblage have been presented in Badanina et al. (2013).

244

245 In-situ Os-isotope data

246

247 'Primary' solitary laurite grains and polyphase laurite-alloy pairs preserved in the chromite cores have
248 $^{187}\text{Os}/^{188}\text{Os}$ values between 0.1214 and 0.1252, with a mean of 0.1242 ± 0.0008 (2 sigma, $n=25$), and $^{187}\text{Re}/^{188}\text{Os}$
249 mainly lower than 0.0003 (Tables 4 and 5). The 'secondary' PGM assemblage is characterized by a similar
250 degree of Os-isotope variations, but with a slightly higher resulting value ($^{187}\text{Os}/^{188}\text{Os}$ values range from 0.1234
251 to 0.1276 with a mean of 0.1245 and a standard deviation of 0.0006, $n=69$, ESM Appendix 1, Table 5). In our
252 data set only two analyses of primary PGM (samples 9-19 and 9-29-1, Table 4) showed less radiogenic Os-
253 isotope values, whereas only two analyses of secondary PGMs (samples 9-100-20 and 9-100-97) deviate from

254 the mean towards more radiogenic Os-isotope values (Tables 4 and 5; ESM Appendix 1; Fig. 8). The osmium
255 isotope results identify a restricted range of broadly similar $^{187}\text{Os}/^{188}\text{Os}$ values for ‘primary’ and ‘secondary’
256 PGM assemblages (Fig. 8, Table 5). Similarly, both model Os-ages (i.e., T_{MA} and T_{RD}) of primary and secondary
257 PGMs, calculated relative to an Enstatite Chondrite Reservoir (ECR) model (Walker et al., 2002a; Shi et al.,
258 2007), are characterized by similar age clusters (550 ± 111 Ma and 508 ± 85 Ma, respectively, Table 5).

260 **Discussion**

262 Compositional and experimental constraints on genesis of polyphase PGM assemblages

263
264 Platinum-group minerals are commonly hosted by podiform chromitites within residual mantle and banded
265 chromitites located in either the transition zone or crustal section of an ophiolite complex. Both types of
266 chromitite are generally well defined based on distinct geological, geochemical and mineralogical features (Lago
267 et al., 1982; Dick and Bullen, 1984; Augé and Johan, 1988; Leblanc, 1991; Melcher, 2000; Malitch et al., 2003b;
268 Prichard et al., 2008; González-Jiménez et al., 2010; Akmaz et al., 2014, among many others).

269 Reports of contrasting PGM assemblages within a particular chromitite pod are rare (Prichard and
270 Tarkian, 1988; Malitch et al., 2001; Badanina et al., 2013a; González-Jiménez et al., 2015). Studies of the
271 Kraubath ophiolite, Austria (Malitch et al., 2003b) and the Guli complex, Russia (Malitch et al., 2002) have
272 shown similar primary PGM assemblages (e.g., laurite, Os-rich iridium and Ir-rich osmium). Elsewhere, laurite
273 is intimately intergrown with either Os-rich iridium, as in the Tiebagi ophiolite, New Caledonia (Augé, 1988),
274 the Samar ophiolite, Philippines (Nakagawa and Franco, 1987), or with Ir-rich osmium, as seen in the Vourinos
275 ophiolite, Greece (Augé, 1985), the Thetford ophiolite, Canada (Corrivaux and Laflamme, 1990) and the Samar
276 ophiolite, Philippines (Nakagawa and Franco, 1987). Complex PGM assemblages (those composed of variety of
277 S- and As-bearing PGM) are thought to indicate chromitites formed in the upper mantle under exceptionally high
278 fluid activity (Torres-Ruiz et al., 1996; Melcher et al., 1997; Garuti et al., 1999).

279 Recent experimental data (Brenan and Andrews, 2001; Andrews and Brenan, 2002) evaluated
280 quantitatively the effects of T and $f(\text{S}_2)$ for laurite + alloy mineral pairs. The compositional results of associated
281 laurite and Os-rich alloys at Harold’s Grave (Badanina et al., 2013a) fit the predicted compositions of
282 experiment W-1200-0.37 that produced laurite and two compositionally distinct alloys (e.g. Ir-rich osmium and
283 Os-rich iridium, both with approximately equal Ru contents, Fig. 3c in Andrews and Brenan, 2002). The analogy
284 with these high temperature experiments (at 1200-1250°C) indicates that the natural laurite–alloy pairs observed
285 were trapped as primary magmatic phases with an ambient $f(\text{S}_2)$ in the range of $10^{-0.39}$ to $10^{-0.07}$ atm (Andrews

286 and Brennan, 2002). The polyphase character of the primary PGM assemblage at Harold's Grave argues against
287 an origin of these PGM by subsolidus exsolution from the chromite host, rather as earlier crystals enclosed by
288 chromite. The origin of the secondary PGM assemblage has been discussed previously (Tarkian and Prichard,
289 1987; Prichard and Tarkian, 1988 among others) and is considered to reflect processes such as in-situ sub-
290 oceanic serpentinisation, alteration during, emplacement and/or post-emplacement regional greenschist
291 metamorphism.

292

293 Constraints on Os-isotope variability in platinum-group minerals

294

295 The early formation of laurite and Os-Ir alloys at high temperatures implies that the original Os-isotope
296 composition of these PGMs reflects the source region in the mantle at the time of formation. Therefore, the low
297 and similar $^{187}\text{Os}/^{188}\text{Os}$ values in laurite and Os-Ir alloys clearly indicate a common near-chondritic mantle
298 source for the PGE. The osmium isotope results of this study display a restricted range of 'unradiogenic'
299 $^{187}\text{Os}/^{188}\text{Os}$ values for intimately intergrown laurite and Os-rich alloy pairs that form a 'primary' PGM
300 assemblage enclosed by chromite (0.12473–0.12488, Fig. 4c). In such pairs the Os isotope signature of the
301 adjacent phases are indistinguishable. Furthermore, this study shows similar 'unradiogenic' $^{187}\text{Os}/^{188}\text{Os}$ values
302 for both primary and secondary PGM assemblages (with a weighted mean of 0.1242 ± 0.0008 and 0.1245 ± 0.0006 ,
303 respectively, Tables 4, 5 and ESM Appendix 1; Fig. 8) that are also consistent (within uncertainty) with the
304 'unradiogenic' $^{187}\text{Os}/^{188}\text{Os}$ value found for the bulk chromitite (0.1240 ± 0.0006). Our Os-isotope compositions
305 are slightly less radiogenic than those of chromitite samples from the same locality previously reported by
306 Walker et al. (2002b) and O'Driscoll et al. (2012) (e.g., 0.12489–0.12554, Table 1). A similarly restricted range
307 of $^{187}\text{Os}/^{188}\text{Os}$ values has been identified in primary and secondary PGM assemblages (with weighted mean
308 $^{187}\text{Os}/^{188}\text{Os}$ of 0.12515 ± 0.00020 and 0.12520 ± 0.00022 , respectively) from a metamorphosed chromitite of the
309 Nurali lhezolite-gabbro massif, South Urals (Table 5, Malitch et al., 2016). At Nurali, the primary Ru-Os
310 sulfides are commonly replaced by a secondary unnamed Ru-Os-Fe-Ir oxide, providing evidence for various
311 stages of desulfurization and oxidation of primary laurite (e.g., with or without laurite relics). As is the case at
312 Harold's Grave, the Os isotope mineral compositions closely match the whole rock Os isotope signature
313 ($^{187}\text{Os}/^{188}\text{Os}=0.12515\pm 0.00020$; Tessalina et al., 2007). Since the PGMs from the secondary assemblage show
314 evidence for alteration, it is possible that their initial $^{187}\text{Os}/^{188}\text{Os}$ could have been modified by reaction with post-
315 magmatic hydrothermal fluids as proposed by González-Jiménez et al. (2012b). The absence of radiogenic
316 $^{187}\text{Os}/^{188}\text{Os}$ values in secondary PGMs, however, suggests that crustal-derived hydrothermal fluids were not
317 supplying radiogenic ^{187}Os . The Os isotope results at Shetland and Nurali are in sharp contrast with the distinctly

1
2
3
4
5
6
7
8
9
10
11
12
13
14
15
16
17
18
19
20
21
22
23
24
25
26
27
28
29
30
31
32
33
34
35
36
37
38
39
40
41
42
43
44
45
46
47
48
49
50
51
52
53
54
55
56
57
58
59
60
61
62
63
64
65

318 different Os isotope compositions observed in primary and secondary PGMs from the metamorphosed
319 chromitites of the Dobromiritsi ophiolite massif, Bulgaria (González-Jiménez et al., 2012b), where the larger
320 range in $^{187}\text{Os}/^{188}\text{Os}$ within the secondary PGMs has been attributed to the interaction of the primary PGMs with
321 a metamorphic-hydrothermal fluid, pointing to open-system behaviour of the Re-Os system in PGMs during
322 metamorphism.

323 The Os-isotope similarity of PGM assemblages and chromitite at Harold's Grave (Tables 1 and 5; Fig.
324 8) and Nurali (Table 5; Tessalina et al., 2007) implies that the whole-rock Os isotope budget is largely controlled
325 by the observed PGM assemblages and possibly by base metal sulfides of similar Os-isotope composition. The
326 observed Os-isotope similarity of PGM assemblages also supports the conclusion that the secondary PGMs have
327 preserved the subchondritic osmium isotope signature of the primary PGMs during alteration, showing no
328 evidence for other crustal source contributions (e.g., suprachondritic material) during later thermal events.
329 Therefore, Os-isotope data documented at Shetland (this study) and Nurali (Malitch et al., 2014; 2016) are
330 consistent with a closed-system behaviour of the Re-Os isotope system in primary and secondary PGMs,
331 preserving mantle signatures during crustal alteration processes. A high resistance of the Os isotope system
332 within PGMs to later thermal events has also been found for Ru-Os-Ir alloys, laurite-erlichmanite and ruarsite-
333 osarsite series PGM from ophiolite- and zoned-type massifs (Kostoyanov, 1998; Hattori and Cabri, 1992;
334 Meibom et al., 2002; Malitch et al., 2003a; Pearson et al., 2007) and from Archaean paleoplacers of the
335 Witwatersrand Basin, South Africa (Malitch and Merkle, 2004; Dale et al., 2010).

336 The highly restricted range of Os-isotope compositions found in both primary and secondary PGM
337 assemblages at IPGE-rich localities in Shetland (Fig. 8, Table 5) and Nurali (Table 5) is at variance with the
338 wider range of Os-isotope compositions recorded in ophiolitic primary PGM assemblages (i.e. containing Ru-
339 Os-Ir alloys, laurite-erlichmanite and ruarsite-osarsite series PGM) from ophiolite-type complexes world-wide
340 (e.g., Kostoyanov, 1998; Rudashevsky et al., 1999; Malitch et al., 2003a; Malitch, 2004; Ahmed et al., 2006; Shi
341 et al., 2007; Nowell et al., 2008; Marchesi et al., 2011; González-Jiménez et al., 2012a; 2014; Badanina et al.,
342 2014; Pašava et al., 2015 and references cited therein). The substantial Os isotope variability seen in the PGMs
343 elsewhere was suggested as representing a long history of melting events of parent ultramafic source-rocks in the
344 mantle (Malitch et al., 2003a; Malitch, 2004), supporting the conclusion that “the Os-isotope system of PGMs
345 records multiple events during the chemical differentiation history of the mantle” (Carlson, 2002) controlled by
346 deep geodynamic processes (Dobretsov and Kirdyashkin, 1998). Likewise, the Os-isotope data at Shetland and
347 Nurali provide no further evidence of small-scale mantle heterogeneity in Os isotopes, as suggested previously
348 (among others, Kostoyanov, 1998; Malitch et al., 2003a; Pearson et al., 2007).

349

350 Os-isotope constraints on Re-Os models of the Earth's mantle and geodynamic implications

351

352 It has been shown (Luck and Allègre, 1991; Walker et al., 1996; Tsuru et al., 2000; Walker et al., 2002b) that
353 Proterozoic and Phanerozoic ophiolites have broadly similar Os isotope signatures consistent with derivation
354 from a chondritic mantle. Previous osmium isotope studies of the SOC were based solely on whole rock data
355 (Walker et al., 2002b; O'Driscoll et al., 2012). Based on isotopic heterogeneity between chromitites and
356 harzburgites O'Driscoll et al. (2012) argued that the former lithology might not be a suitable proxy for the
357 average $^{187}\text{Os}/^{188}\text{Os}$ composition of the bulk convecting upper mantle. Since the geological history of the
358 Shetland ophiolite is reasonably well-known (Spray, 1988; Flinn et al., 1991; Flinn, 2000; 2001; 2007; Flinn and
359 Oglethorpe 2005; Cutts et al., 2011, among others) the Os-isotope data can be used to constrain the long-term
360 Re-Os evolution of the Earth's upper mantle. Different mantle evolution curves were defined as follows. The
361 Carbonaceous Chondrite reservoir (CCR) curve assumes that the Earth's mantle has an Os isotopic composition
362 and Re/Os similar to that of carbonaceous chondrites ($^{187}\text{Os}/^{188}\text{Os}_{\text{CC}}=0.1262\pm 0.0006$, $^{187}\text{Re}/^{188}\text{Os}_{\text{CC}}=0.392$
363 ± 0.015 (Walker et al., 2002a). The Enstatite Chondritic Reservoir (ECR) curve is calculated using a present-day
364 $^{187}\text{Os}/^{188}\text{Os}$ value of 0.1281 ± 0.0004 and $^{187}\text{Re}/^{188}\text{Os}=0.421\pm 0.013$ as measured in enstatite chondrites (Walker et
365 al., 2002a). The Primitive Upper Mantle (PUM) curve has a present day $^{187}\text{Os}/^{188}\text{Os}=0.1296\pm 0.0008$ and
366 $^{187}\text{Re}/^{188}\text{Os}=0.42$. These estimates were obtained through linear regression through suites of mantle-derived
367 peridotite xenoliths and orogenic peridotites sampling mainly the Proterozoic to Phanerozoic subcontinental
368 upper mantle (Meisel et al., 2001b). By comparing the Os-isotope composition of chromitite and distinct PGM
369 assemblages and the independent chronological data available for the SOC we can distinguish between the
370 various proposed mantle evolution curves (Fig. 9) following the approach of Shi et al. (2007). As is shown in
371 Fig. 9 the CCR model yields an unrealistically young age (i.e. ca. 300 Ma), much younger than the emplacement
372 age of the ophiolite. The PUM model would require melting (or depletion) at 790 Ma, but that is older than the
373 opening of Iapetus ocean system, so also seems unlikely. The ECR model would fit with melting at c 510-560
374 Ma, which is a reasonable match to the other available dating for the SOC, so seems most likely with the
375 available data.

376 Using an ECR model we obtain Os-model ages ($T_{\text{MA}}^{\text{ECR}} \sim T_{\text{RD}}^{\text{ECR}}$) for PGM assemblages and chromitite
377 within a range of ca. 508 and 580 Ma, respectively. These estimates would agree within the ECR model
378 uncertainty (Fig. 9) with the plagiogranite zircon U-Pb ages (492 ± 3 Ma, Spray and Dunning, 1991) and the K-Ar
379 ages of hornblende (465-479 Ma, Spray 1988) determined in amphibolites found in Unst and Fetlar that are
380 thought to be the remnants of dynamo-metamorphic sole from hot obduction (Williams and Smyth, 1973;
381 Prichard, 1985), albeit one complicated by later tectonic and/or magmatic activity. Thus the unradiogenic

382 $^{187}\text{Os}/^{188}\text{Os}$ isotope systematics of laurite-dominated assemblages in this study record melt depletion events that
383 are slightly older than final crystallisation (i.e., of zircons from plagiogranites in late stage veins in the gabbro
384 unit) and the subsequent ophiolite emplacement into crustal levels (i.e. metamorphic sole formation). Therefore,
385 the ages implied by our modelling of these new Os isotope results are also consistent with a supra-subduction
386 zone origin of the SOC, which would be followed relatively rapidly by obduction.

387

388 **Conclusions**

389

390 1. Two distinct PGM assemblages (primary and secondary), each dominated by laurite and Os-rich alloy, have
391 been observed at Harold's Grave in the Shetland Ophiolite Complex, below the transition zone harzburgite and
392 petrological Moho. The primary PGM assemblage formed early (together with chromite), whereas the secondary
393 PGM assemblage is likely to reflect alteration processes such as *in-situ* serpentinization, alteration during
394 emplacement or regional greenschist metamorphism.

395 2. The osmium isotope results reveal broadly similar 'unradiogenic' $^{187}\text{Os}/^{188}\text{Os}$ values for both primary and
396 secondary PGM assemblages which are similar to that of the chromitite host, supporting the conclusion that the
397 'secondary' PGMs preserved the subchondritic osmium isotope signature of the 'primary' PGMs. This implies
398 that the whole-rock Os isotope budget is largely controlled by the laurite-dominant assemblages.

399 3. Os-isotope data for chromitite and the associated PGM assemblages support an ECR model for the convective
400 upper mantle as defined by Walker et al. (2002b) and are consistent with origin of the complex as a Caledonian
401 ophiolite formed in a supra-subduction zone shortly before obduction.

402 4. The results demonstrate that PGE-enriched ophiolite chromitites can still preserve primitive mantle Os isotope
403 compositions, despite complex post-magmatic alteration histories.

404

405 **Acknowledgements**

406

407 This paper is a contribution to the project #12-05-01166-a to I.Yu. Badanina funded by the Russian Foundation
408 for Basic Research. The analytical data at CCFS/GEMOC were obtained using instrumentation funded by DEST
409 Systemic Infrastructure Grants, ARC LIEF, NCRIS/AuScope, industry partners and Macquarie University. The
410 chromitite sample used was originally collected by RAL as part of the Mining Industry Research Organisation
411 research programme contract RC48. Prof. S.Y. O'Reilly, Prof. W.L. Griffin, Dr. J.M. González-Jiménez, Dr.
412 N.J. Pearson, Dr. S.A. Junk, Dr. V.V. Knauf and Dr. H. Prichard are thanked for valuable discussions. This is
413 contribution 679 from the ARC Centre of Excellence for Core to Crust Fluid Systems

414 (<http://www.ccfs.mq.edu.au>) and 1042 in the GEMOC Key Centre (<http://www.gemoc.mq.edu.au>). The paper
415 has benefitted from constructive comments of three anonymous reviewers. Careful editorial handling of Editor-
416 in-chief Dr. Franco Pirajno is greatly appreciated.

417

418 **References**

419 Ahmed, A.H., Hanghøj, K., Kelemen, P.B., Hart, S.R., Arai, S., 2006. Osmium isotope systematics of the
420 Proterozoic and Phanerozoic ophiolitic chromitites: in-situ ion probe analysis of primary Os-rich PGM.
421 Earth and Planetary Science Letters 245, 777-791.

422 Akmaz, R.M., Uysal, I., Saka, S., 2014. Compositional variations of chromite and solid inclusions in ophiolitic
423 chromitites from the southeastern Turkey: Implications for chromitite genesis. Ore Geology Reviews
424 58, 208-224.

425 Alard, O., Griffin, W.L., Pearson, N.J., Lorand, J.-P., O'Reilly, S.Y., 2002. New insights into the Re-Os
426 systematics of sub-continental lithospheric mantle from in situ analysis of sulphides. Earth and
427 Planetary Science Letters 203, 651-663.

428 Alard, O., Luguët, A., Pearson, N.J., Griffin, W.L., Lorand, J.-P., Gannoun, A., Burton, K.W., O'Reilly, S.Y.,
429 2005. In *situ* Os isotopes in abyssal peridotites bridge the isotopic gap between MORBs and their source
430 mantle. Nature 436, 1005-1008.

431 Andrews, D.R.A., Brenan, J.M., 2002. Phase-equilibrium constraints on the magmatic origin of laurite and Os-Ir
432 alloy. Canadian Mineralogist 40, 1705-1716.

433 Augé, T., 1985. Platinum-group-mineral inclusions in ophiolitic chromite from the Vourinos Complex, Greece.
434 Canadian Mineralogist 23, 163-171.

435 Augé, T., 1988. Platinum-group minerals in the Tiebaghi and Vourinos ophiolitic complexes: genetic
436 implications. Canadian Mineralogist 26, 177-192.

437 Augé, T., Johan, Z., 1988. Comparative study of chromite deposits from Troodos, Vourinos, North Oman and
438 New Caledonia ophiolites. In: Boissonnas, J., Omenetto, P. (Eds.), Mineral Deposits within the
439 European Community. Springer, Berlin, Heidelberg, Special Publication of the Society for Geology
440 Applied to Mineral Deposits, 267-288.

441 Badanina, I.Yu., Malitch, K.N., Lord, R.A., Meisel, T.C., 2013a. Origin of primary PGM assemblage in
442 chromitite from a mantle tectonite at Harold's Grave (Shetland Ophiolite Complex, Scotland).
443 Mineralogy and Petrology 107, 963-970.

444 Badanina, I.Yu., Malitch, K.N., Murzin, V.V., Khiller, V.V., Glavatskikh, S. P., 2013b. Mineralogical and
445 geochemical particularities of PGE mineralization of the Verkh-Neivinsk dunite-harzburgite massif
446 (Middle Urals, Russia). Proceedings of the Institute of Geology and Geochemistry UB RAS 160, 188-
447 192 (in Russian).

- 448 Badanina, I.Yu., Malitch, K.N., Lord, R.A., Belousova, E.A., Griffin, W.L., Meisel, T.C., Murzin, V.V.,
449 Pearson, N.J., O'Reilly, S.Y., 2014. Mineral chemistry and isotopic composition of ophiolitic Os-rich
450 alloys and Ru-Os sulfides: synthesis of new data. In: Anikina, E.V. et al. (Eds.), 12th International
451 Platinum Symposium Abstracts. Institute of Geology and Geochemistry UB RAS, Yekaterinburg,
452 Russia, 289-290.
- 453 Barnes, S.J., Naldrett, A.J., Gorton, M.P., 1985. The origin of the fractionation of platinum-group elements in
454 terrestrial magmas. *Chemical Geology*, 53, 303-323.
- 455 Becker, H., Shirey, S.B., Carlson, R.W., 2001. Effects of melt percolation on the Re-Os systematics of
456 peridotites from a Paleozoic convergent plate margin. *Earth and Planetary Science Letters* 188, 107-
457 121.
- 458 Brandon, A.D., Creaser, R.A., Shirey, S.B., Carlson, R.W., 1996. Osmium recycling in subduction zones.
459 *Science* 272, 861-864.
- 460 Brandon, A.D., Walker, R.J., Puchtel, I.S., 2006. Platinum-osmium isotope evolution of the Earth's mantle: constraints
461 from chondrites and Os-rich alloys. *Geochimica et Cosmochimica Acta* 70, 2093-2103.
- 462 Brenan, J.M., Andrews, D., 2001. High-temperature stability of laurite and Ru–Os–Ir alloy and their role in PGE
463 fractionation in mafic magmas. *Canadian Mineralogist* 39, 341-360.
- 464 Brough, C.P., Prichard, H.M., Neary, C.R., Fisher, P.C., McDonald, I., 2015. Geochemical variations within
465 podiform chromitite deposits in the Shetland ophiolite: Implications for petrogenesis and PGE
466 concentration. *Economic Geology* 110, 187-208.
- 467 Burton, K.W., Schiano, P., Birck, J.-L., Allègre, C.J., 1999. Osmium isotope disequilibrium between mantle
468 minerals in a spinel-lherzolite. *Earth and Planetary Science Letters* 172, 311-322.
- 469 Burton, K.W., Gannoun, A., Birck, J.L., Allègre, C.J., Schiano, P., Clocchiatti, R., Alard, O., 2002. The
470 compatibility of rhenium and osmium in natural olivine and their behaviour during mantle melting and
471 basalt genesis. *Earth and Planetary Science Letters* 198, 63-76.
- 472 Carlson, R.W., 2002. Osmium remembers. *Science* 296, 475-477.
- 473 Carlson, R.W., 2005. Application of the Pt–Re–Os isotopic systems to mantle geochemistry and geochronology.
474 *Lithos* 82, 249-272.
- 475 Corrivaux, L., Laflamme, J.H.G., 1990. Minéralogie des éléments du groupe du platine dans les chromitites de
476 l'ophiolite de Thetford Mines, Québec. *Canadian Mineralogist* 28, 579-595.
- 477 Cutts, K.A., Hand, M., Kelsey, D.E., Strachan, R.A., 2011. P-T constraints and timing of Barrovian
478 metamorphism in the Shetland Islands, Scottish Caledonides: implications for the structural setting of
479 the Unst ophiolite *Journal of the Geological Society* 168, 1265-1284.

- 480 Dale, C.W., Pearson, D.G., Nowell, G.M., Parman, S.W., Oberthur, T., Malitch K.N., 2010. Os isotopes in
481 Witwatersrand platinum-group alloys: implications for ancient mantle melting events and the timing of
482 gold formation. *Geochimica et Cosmochimica Acta* 74 (12) Suppl. 1, A203.
- 483 Derbyshire, E.J., O'Driscoll, B., Lenaz, D, Gertisser, R., Kronz, A., 2013. Compositionally heterogeneous
484 podiform chromitite in the Shetland Ophiolite Complex (Scotland): Implications for chromitite
485 petrogenesis and late-stage alteration in the upper mantle portion of a supra-subduction zone ophiolite.
486 *Lithos* 162-163, 279-300.
- 487 Dick, H.J.B., Bullen, T., 1984. Chromian spinel as a petrogenetic indicator in abyssal and alpine-type peridotites
488 and spatially associated lavas. *Contributions to Mineralogy and Petrology* 86, 54-76.
- 489 Dobretsov, N.L., Kirdyashkin, A.G., 1998. Deep-level geodynamics. Swets and Zeitlinger, Rotterdam. 328 p.
- 490 Flinn, D., 1985. The Caledonides of Shetland. In: Gee, D.G., Sturt, B.A. (Eds.), *The Caledonide Orogen -*
491 *Scandinavia and related areas.* Wiley and Sons, 1158-1171.
- 492 Flinn, D., 1996. The Shetland Ophiolite Complex: field evidence for the intrusive emplacement of the 'cumulate'
493 layers. *Scottish Journal of Geology* 32, 151-158.
- 494 Flinn, D., 2000. The architecture of the Shetland Ophiolite Complex. *Scottish Journal of Geology* 36, 123-135.
- 495 Flinn, D., 2001. The basic rocks of the Shetland Ophiolite Complex and their bearing on its genesis. *Scottish*
496 *Journal of Geology* 37, 79-96.
- 497 Flinn, D. 2007. The Dalradian rocks of Shetland and their implications for the plate tectonics of the northern
498 Iapetus. *Scottish Journal of Geology* 43, 125-142.
- 499 Flinn, D., Oglethorpe, R.D., 2005. A history of the Shetland Ophiolite Complex. *Scottish Journal of Geology*
500 141-148.
- 501 Flinn, D., Frank, P.L., Brook, M., Pringle, I.R., 1979. Basement-cover relations in Shetland. In: Harris, A.,
502 Holland, C.H., Leake, B.E. (Eds.), *The Caledonides of the British Isles Reviewed*, Geological Society,
503 London, Spec. publ. 8, 109-115.
- 504 Flinn, D., Miller, J.A., Roddam, D., 1991. The age of the Norwick hornblendic schists of Unst and Fetlar and the
505 obduction of the Shetland ophiolite. *Scottish Journal of Geology* 27, 11-19.
- 506 Garson, M.S., Plant, J., 1973. Alpine type ultramafic rocks and episodic mountain building in the Scottish
507 Highlands. *Nature (Phys. Sci.)* 242, 34-38.
- 508 Garuti, G., Zaccarini, F., Moloshag, V., Alimov, V., 1999. Platinum-group minerals as indicators of sulfur
509 fugacity in ophiolitic upper mantle: an example from chromitites of the Rai-Iz ultramafic complex,
510 Polar Urals, Russia. *Canadian Mineralogist* 37, 1099-1115.
- 511 González-Jiménez, J.M., Gervilla, F., Proenza, J.A., Augé, T., Kerestedjian, T., 2010. Distribution of platinum-
512 group minerals in ophiolitic chromitites. *Transactions of the Institutions of Mining and Metallurgy,*
513 *Section B: Applied Earth Science* 118 (3-4), 101-110.

- 514 González-Jiménez, J.M., Gervilla, F., Griffin, W.L., Proenza, J.A., Augé, T., O'Reilly, S.Y., Pearson, N.J.,
515 2012a. Os-isotope variability within sulfides from podiform chromitites. *Chemical Geology* 291, 224-
516 235.
- 517 González-Jiménez, J.M., Griffin, W.L., Gervilla, F., Kerestedjian, T.N., O'Reilly, S.Y., Proenza, J.A., Pearson,
518 N.J., Sergeeva, I., 2012b. Metamorphism disturbs the Re-Os signatures of platinum-group minerals in
519 ophiolite chromitites. *Geology* 40, 659-662.
- 520 González-Jiménez, J.M., Griffin, W.L., Gervilla, F., Proenza, J.A., O'Reilly, S.Y., Pearson, N.J., 2014.
521 Chromitites in ophiolites: how, where, when, why? Part I. A review and new ideas on the origin and
522 significance of platinum-group minerals. *Lithos* 189, 127-139.
- 523 González-Jiménez, J.M., Locmelis, M., Belousova, E., Griffin, W., Gervilla, F., Kerestedjian, T.N., O'Reilly,
524 S.Y., Pearson, N.J., Sergeeva, I., 2015. Genesis and tectonic implications of podiform chromitites in the
525 metamorphosed ultramafic massif of Dobromiritsi (Bulgaria). *Gondwana Research* 27, 555-574.
- 526 Gunn, A.G., Styles, M.T., 2002. Platinum-group element occurrences in Britain: magmatic, hydrothermal and
527 supergene. *Applied Earth Science: IMM Transactions section B* 111, 2-14.
- 528 Harris, D.C., Cabri, L.J., 1991. Nomenclature of platinum-group-element alloys: Review and revision.
529 *Canadian Mineralogist* 29, 231-237.
- 530 Hart, S.R., Ravizza, G.E., 1996. Os partitioning between phases in lherzolite and basalt. In: Basu, A., Hart, S.R.
531 (Eds.), *Earth processes: reading the isotopic code*. Geophys. Monogr. Ser. 95. AGU, Washington,
532 USA (pp. 123-134).
- 533 Hattori, K., Hart, S.R., 1991. Osmium-isotope ratios of platinum-group minerals associated with ultramafic
534 intrusions: Os-isotopic evolution of the oceanic mantle. *Earth and Planetary Science Letters* 107, 499-
535 514.
- 536 Hattori, K., Cabri, L.J., 1992. Origin of platinum-group mineral nuggets inferred from an osmium-isotope study.
537 *Canadian Mineralogist* 30, 289-301.
- 538 Junk, S.A., 2001. Ancient artefacts and modern analytical techniques - Usefulness of laser ablation ICP-MS
539 demonstrated with ancient gold coins. *Nuclear Instruments and Methods in Physics Research B* 181,
540 723-727.
- 541 Knauf, V.V., 1996. On the methodological background of mineralogical investigations. *Zapiski Vserossiiskogo*.
542 *Mineralogicheskogo Obshchestva* 125, 109-113 (in Russian).
- 543 Kostoyanov, A.I., 1998. Model Re-Os ages of platinum-group minerals. *Geologiya Rudnykh Mestorozhdenii* 40,
544 545-550 (in Russian).
- 545 Lago, B.L., Rabinowicz, M., Nicolas, A., 1982. Podiform chromite ore bodies: a genetic model. *Journal of*
546 *Petrology* 23, 103-125.
- 547 Leblanc, M., 1991. Platinum-group elements and gold in ophiolitic complexes: Distribution and fractionation
548 from mantle to oceanic floor. In: Peters, T.J., Nicolas, A., Coleman, R.G. (Eds.), *Ophiolite Genesis and*

- 549 Evolution of the Oceanic Lithosphere. Ministry of Petroleum and Minerals, Sultanate of Oman, pp. 231-
550 260.
- 1
2 551 Le Roux, V., Bodinier, J.-L., Alard, O., O'Reilly, S.Y., Griffin W.L., 2009. Isotopic decoupling during porous
3
4 552 melt flow: A case study in the Lherz peridotites. *Earth and Planetary Science Letters* 279, 76-85.
- 5
6 553 Lorand, J.-P., Alard, O., 2001. Platinum-group element abundances in the upper mantle: new constraints from in
7
8 554 situ and whole-rock analyses of Massif Central xenoliths (France). *Geochimica et Cosmochimica Acta*
9
10 555 65, 2789-2806.
- 11 556 Lord, R.A., 1991. Platinum-group element mineralisation in the Shetland ophiolite complex. Ph.D. thesis, Open
12
13 557 University, Milton Keynes, U.K., 422 pp.
- 14
15 558 Lord, R.A., Prichard, H.M., 1997. Exploration and origin of stratigraphically controlled platinum-group element
16
17 559 mineralization in crustal-sequence ultramafics, Shetland ophiolite complex. *Transactions of the*
18
19 560 *Institutions of Mining and Metallurgy, Section B: Applied Earth Science* 106: B179-B193.
- 20
21 561 Lord, R.A., Prichard, H.M., Neary, C.R., 1994. Magmatic platinum-group element concentrations and
22
23 562 hydrothermal upgrading in Shetland ophiolite complex. *Transactions of the Institutions of Mining and*
24
25 563 *Metallurgy, Section B*, 103, 87-106.
- 26
27 564 Luck, J.-M., Allègre, C.J., 1991. Osmium isotopes in ophiolites. *Earth and Planetary Science Letters* 107, 406-
28
29 565 415.
- 30
31 566 Luguet, A., Behrens, M., Pearson D.G., Konig, S., Herwartz, D., 2015. Significance of the whole rock Re-Os
32
33 567 ages in cryptically and modally metasomatised cratonic peridotites: Constraints from HSE-Se-Te
34
35 568 systematics. *Geochimica et Cosmochimica Acta* 164, 441-463.
- 36
37 569 Malitch, K.N., 2004. Osmium isotope constraints on contrasting sources and prolonged melting in the
38
39 570 Proterozoic upper mantle: evidence from ophiolitic Ru-Os sulfides and Ru-Os-Ir alloys. *Chemical*
40
41 571 *Geology* 208, 157-173.
- 42
43 572 Malitch, K.N., Anikina, E.V., Badanina, I.Yu., Belousova, E.A., Griffin, W.L., Khiller, V.V., Pearson, N.J.,
44
45 573 Pushkarev, E.V., O'Reilly, S.Y., 2014. Closed-system behaviour of the Re-Os isotope system in
46
47 574 primary and secondary PGM assemblages: evidence from the Nurali ultramafic complex (Southern
48
49 575 Urals, Russia). In: Anikina, E.V. et al. (Eds.), 12th International Platinum Symposium Abstracts.
50
51 576 Institute of Geology and Geochemistry UB RAS, Yekaterinburg, Russia, 299-300.
- 52
53 577 Malitch, K.N., Anikina, E.V., Badanina, I.Yu., Belousova, E.A., Pushkarev, E.V., Khiller, V.V., 2016.
54
55 578 Composition and osmium isotope systematics of primary and secondary platinum-group mineral
56
57 579 assemblages from Mg-bearing chromitite of the Nurali lherzolite massif (Russia). *Geology of Ore*
58
59 580 *Deposits* 58 (1), 1-20 (in press).
- 60
61 581 Malitch, K.N., Augé, T., Badanina, I.Yu., Goncharov, M.M., Junk, S.A., Pernicka, E., 2002. Os-rich nuggets
62
63 582 from Au-PGE placers of the Maimecha-Kotui Province, Russia: a multi-disciplinary study. *Mineralogy*
64
65 583 *and Petrology* 76, 121-148.

- 584 Malitch, K.N., Junk, S.A., Thalhammer, O.A.R., Melcher, F., Knauf, V.V., Pernicka, E., Stumpfl, E.F. 2003a.
585 Laurite and ruarsite from podiform chromitites at Kraubath and Hochgrussen, Austria: new insights
586 from osmium isotopes. *Canadian Mineralogist* 41, 331-352.
- 587 Malitch, K.N., Melcher, F., Mühlhans, H., 2001. Palladium and gold mineralization in podiform chromitite at
588 Kraubath, Austria. *Mineralogy and Petrology* 73, 247-277.
- 589 Malitch, K.N., Merkle, R.K.W., 2004. Ru-Os-Ir-Pt and Pt-Fe alloys from the Evander Goldfield (Witwatersrand
590 Basin, South Africa): detrital origin inferred from compositional and osmium isotope data. *Canadian*
591 *Mineralogist* 42, 631-650.
- 592 Malitch, K.N., Thalhammer, O.A.R., Knauf, V.V., Melcher, F., 2003b. Diversity of platinum-group mineral
593 assemblages in banded and podiform chromitite from the Kraubath ultramafic massif, Austria: evidence
594 for an ophiolitic transition zone? *Mineralium Deposita* 38, 282-297.
- 595 Marchesi, C., González-Jiménez, J.M., Gervilla, F., Griffin, W.L., O'Reilly, S.Y., Proenza, J.A., Pearson, N.J.,
596 2011. In situ Re-Os isotopic analysis of platinum-group minerals from the Mayarí-Cristal ophiolitic
597 massif (Mayarí-Baracoa Ophiolitic Belt, eastern Cuba): implications for the origin of Os-isotope
598 heterogeneities in podiform chromitites. *Contributions to Mineralogy and Petrology* 161, 977-990.
- 599 Martin, C.E., Papanastassiou, D.A., Wasserburg, G.J., Peach, C.L., 1993. Os isotopic composition of sulfide
600 globules from MORB. *EOS (Transactions, American Geophysical Union)* 74, 121.
- 601 McDonough, W.F., Sun, S.S., 1995. The composition of the Earth. *Chemical Geology* 120, 223-253.
- 602 Melcher, F., 2000. Chromite and platinum-group elements as indicators of mantle petrogenesis. Unpubl. Habil.
603 thesis. Mining University Leoben, 202 pp.
- 604 Melcher, F., Grum, W., Simon, G., Thalhammer, T.V., Stumpfl, E.F., 1997. Petrogenesis of the ophiolitic giant
605 chromite deposits of Kempirsai, Kazakhstan: a study of solid and fluid inclusions in chromite. *Journal*
606 *of Petrology* 38, 1419-1458.
- 607 Meibom, A., Sleep, N.H., Chamberlain, C.P., Coleman, R.G., Frei, R., Hren, M.T., Wooden, J.L., 2002. Re-Os
608 isotopic evidence for long-lived heterogeneity and equilibration processes in the Earth's upper mantle.
609 *Nature* 419, 705-708.
- 610 Meisel, T., Fellner, N., Moser, J., 2003. A simple procedure for the determination of platinum-group elements
611 and rhenium (Ru, Rh, Pd, Re, Os, Ir and Pt) using ID-ICP-MS with an inexpensive on-line- matrix
612 separation in geological and environmental materials. *Journal of Analytical Atomic Spectrometry* 18,
613 720-726.
- 614 Meisel, T., Moser, J., Fellner, N., Wegscheider, W., Schoenberg, R., 2001a. Simplified method for the
615 determination of Ru, Pd, Re, Os, Ir and Pt in chromitites and other geological materials by isotope
616 dilution ICPMS and acid digestion. *Analyst* 126, 322-328.
- 617 Meisel, T., Walker, R.J., Irving, A.J., Lorand, J.-P., 2001b. Osmium isotopic composition of mantle xenoliths: A
618 global perspective. *Geochimica et Cosmochimica Acta* 65, 1311-1323.

- 619 Nakagawa, M., Franko, H.A., 1997. Placer Os-Ir-Ru alloys and sulfides: indicators of sulfur fugacity in an
620 ophiolite. *Canadian Mineralogist* 35, 1441-1452.
- 621 Nowell, G.M., Pearson, D.G., Parman, S.W., Luguët, A., Hanski, E., 2008. Precise and accurate $^{186}\text{Os}/^{188}\text{Os}$ and
622 $^{187}\text{Os}/^{188}\text{Os}$ measurements by Multi-collector Plasma Ionisation Mass Spectrometry, part II: Laser
623 ablation and its application to single-grain Pt–Os and Re–Os geochronology. *Chemical Geology* 248,
624 394-426.
- 625 O'Driscoll, B., James, M.D., Day, J.M.D., Walker, R.J., Daly, J.S., McDonough, W.F., Piccoli, P.M., 2012.
626 Chemical heterogeneity in the upper mantle recorded by peridotites and chromitites from the Shetland
627 Ophiolite Complex, Scotland. *Earth and Planetary Science Letters* 333-334, 226-237.
- 628 O'Reilly, S.Y., Griffin, W.L., 2012. Mantle metasomatism. In: Harlov, D.E., Austrheim, H. (Eds.),
629 *Metasomatism and the Chemical Transformation of Rock: Lecture Notes in Earth System Sciences*.
630 Berlin, Springer-Verlag, pp. 467-528.
- 631 Paliulionyte, V., Meisel, T., Ramminger, P., Kettisch, P., 2006. High pressure asher digestion and an isotope
632 dilution-ICP-MS method for the determination of platinum-group element concentrations in chromitite
633 reference materials CHR-Bkg, GAN Pt-1 and HHH. *Geostandards and Geoanalytical Research* 30, 87-
634 96.
- 635 Pašava, J., Malec, J., Griffin, W.L., González-Jiménez, J.M., 2015. Re–Os isotopic constraints on the source of
636 platinum-group minerals (PGMs) from the Vestřev pyrope-rich garnet placer deposit, Bohemian Massif.
637 *Ore Geology Reviews* 68, 117-126.
- 638 Pearson, N.J., Alard, O., Griffin, W.L., Jackson, S.E., O'Reilly, S.Y., 2002. In situ measurement of Re-Os
639 isotopes in mantle sulfides by laser ablation multicollector-inductively coupled plasma mass
640 spectrometry: Analytical methods and preliminary results. *Geochimica et Cosmochimica Acta* 66, 1037-
641 1050.
- 642 Pearson, D.G., Parman, S.W., Nowell, G.M., 2007. A link between large mantle melting events and continent
643 growth seen in osmium isotopes. *Nature* 449, 202-205.
- 644 Prichard, H.M., 1985. The Shetland Ophiolite. In: Gee, D.G., Sturt, B.A. (Eds.), *The Caledonide Orogen:*
645 *Scandinavia and related areas*. Wiley and Sons. Ltd. 2, 1173-1184.
- 646 Prichard, H.M., Ixer, R.A., Lord, R.A., Maynard, J., Williams, N., 1994. Assemblages of platinum-group
647 minerals and sulfides in silicate lithologies and chromite-rich rocks within the Shetland Ophiolite.
648 *Canadian Mineralogist* 32, 271-294.
- 649 Prichard, H.M., Lord, R.A., 1988. The Shetland ophiolite: evidence for a supra-subduction zone origin and
650 implications for platinum-group element mineralization. In: Boissonnas J., Omenetto P. (Eds.), *Mineral*
651 *Deposits within the European Community*. Special Publication No. 6 of the Society for Geology
652 *Applied to Mineral Deposits*, Springer-Verlag, Berlin, 289-302.

- 653 Prichard, H.M., Lord, R.A., 1993. An overview of the PGE concentrations in the Shetland ophiolite complex. In:
654 Prichard, H.M., Alabaster, T., Harris, N.B.W., Neary, C.R. (Eds.), *Magmatic processes and plate*
655 *tectonics*, Special Publication of the Geological Society of London 76, 273-294.
- 656 Prichard, H.M., Lord, R.A., Neary, C.R., 1996. A model to explain the occurrence of platinum- and palladium-
657 rich ophiolite complexes. *Journal of the Geological Society* 153, 323-328.
- 658 Prichard, H.M., Neary, C.R., Fisher, P.C., O'Hara, M.J., 2008. PGE-rich podiform chromitites in the Al'Ays
659 Ophiolite Complex, Saudi Arabia: An example of critical mantle melting to extract and concentrate
660 PGE. *Economic Geology* 103, 1507-1529.
- 661 Prichard, H.M., Neary, C.R., Potts, P.J., 1986. Platinum-group minerals in the Shetland ophiolite. In: Gallagher,
662 M.J., Ixer, R.A., Neary, C.R., Prichard, H.M. (Eds.), *Metallogeny of Basic and Ultrabasic Rocks*. Inst.
663 *Mining Metall.* London, 395-414.
- 664 Prichard, H.M., Tarkian, M., 1988. Platinum and palladium minerals from two PGE-localities in the Shetland
665 ophiolite complex. *Canadian Mineralogist* 26, 979-990.
- 666 Rosman, K.J.R., Taylor, P.D.P., 1998. Isotopic compositions of the elements 1997. *Pure and Applied Chemistry*
667 70, 217-235.
- 668 Rudashevsky, N.S., Garuti, G., Andersen, J.C.Ø., Kretser, Y.L., Rudashevsky, V.N., Zaccarini, F., 2002.
669 Separation of accessory minerals from rocks and ores by hydroseparation (HS) technology: method and
670 application to CHR-2 chromitite, Niquelandia, Brazil. *Transactions, Institution of Mining and*
671 *Metallurgy, Proceedings Australasian Institute Mining Metallurgy (Sect. B: Applied earth science)* 111,
672 B87-B94.
- 673 Rudashevsky, N.S., Kostoyanov, A.I., Rudashevsky, V.N., 1999. Mineralogical and isotope evidences of origin
674 of the Alpine-type massifs (the Ust'-Bel'sky massif, Koryak Highland, as an example). *Zapiski*
675 *Vserossiiskogo. Mineralogicheskogo Obshchestva* 128, 11-28 (in Russian).
- 676 Rudnick, R.L., Walker, R.J., 2009. Interpreting ages from Re-Os isotopes in peridotites. *Lithos* 112, 1083-1095.
- 677 Sambridge, M., Lambert, D.D., 1997 Propagating errors in decay equations: examples from the Re-Os isotopic
678 system. *Geochimica et Cosmochimica Acta*, 61, 3019-3024.
- 679 Shi, R., Alard, O., Zhi, X., O'Reilly, S.Y., Pearson, N.J., Griffin, W.L., Zhang, M., Chen, X., 2007. Multiple
680 events in the Neo-Tethyan oceanic upper mantle: Evidence from Ru-Os-Ir alloys in the Luobusa and
681 Dongqiao ophiolitic podiform chromitites, Tibet. *Earth and Planetary Science Letters* 261, 33-48.
- 682 Shirey, S.B., Walker, R.J., 1998. The Re-Os isotope system in cosmochemistry and high-temperature
683 geochemistry. *Annual Review of Earth and Planetary Sciences* 26, 423-500.
- 684 Smoliar, M.I., Walker, R.J., Morgan, J.W., 1996. Re-Os ages of group IIA, IIIA, IVA, and IVB meteorites.
685 *Science* 271, 1099-1102.
- 686 Spray, J.G., 1988. Thrust related metamorphism beneath the Shetland Islands ocean fragment, north-east
687 Scotland. *Canadian Journal of Earth Sciences* 25, 1770-1776.

- 688 Spray, J.G., Dunning, G.R., 1991. A U/Pb age for the Shetland Islands oceanic fragment, Scottish Caledonides:
689 evidence from anatectic plagiogranites in 'layer 3' shear zones. *Geological Magazine* 128, 667-671.
- 690 Standish, J.J., Hart, S.R., Blusztajn, J., Dick, H.J.B., Lee, K.L., 2001. Abyssal peridotite osmium isotopic
691 compositions from Cr-spinel. *Geochemistry Geophysics Geosystems* 3 (1), 10.1029/2001GC000161,
692 2002.
- 693 Tarkian, M., Prichard, H., 1987. Irarsite-hollingworthite solid solution series and other associated Os-, Ir- and
694 Rh-bearing PGM's from the Shetland ophiolite complex. *Mineralium Deposita* 22, 178-184.
- 695 Tessalina, S.G., Bourdon, B., Gannoun, A., Campas, F., Birck, J.-L., Allegre, C.J., 2007. Complex proterozoic to
696 paleozoic history of the upper mantle recorded in the Urals lherzolite massifs by Re-Os and Sm-Nd
697 systematics. *Chemical Geology* 240, 61-84.
- 698 Torres-Ruiz, J., Garuti, G., Gazzotti, M., Gervilla, F., Fenoll Hach-Ali, P., 1996. Platinum-group minerals in
699 chromitites from the Ojen lherzolite massif (Serrania de Ronda, Betic Cordillera, Southern Spain).
700 *Mineralogy and Petrology* 56, 25-50.
- 701 Tsuru, A., Walker, R.J., Kontinen, A., Peltonen, P., Hanski, E., 2000. Re-Os isotopic systematics of the 1.95 Ga
702 Jormua ophiolite complex, northeastern Finland. *Chemical Geology* 164, 123-141.
- 703 Walker, R.J., Hanski, E., Vuollo, J., Liipo, J., 1996. The Os isotopic composition of Proterozoic upper mantle:
704 evidence from the Outokumpu ophiolite, Finland. *Earth and Planetary Science Letters* 141, 161-173.
- 705 Walker, R.J., Horan, M.F., Morgan, J.W., Becker, H., Grossman, J.N., Rubin, A.E., 2002a. Comparative ¹⁸⁷Re-
706 ¹⁸⁷Os systematics of chondrites: implications regarding early solar system processes. *Geochimica et*
707 *Cosmochimica Acta* 66, 4187-4201.
- 708 Walker, R.J., Prichard, H.M., Ishiwatari, A., Pimentel, M., 2002b. The osmium isotopic composition of
709 convecting upper mantle deduced from ophiolite chromites. *Geochimica et Cosmochimica Acta* 66,
710 329-345.
- 711 Williams, H., Smyth, W.R., 1973. Metamorphic aureoles beneath ophiolite suites and Alpine peridotites: tectonic
712 implications with west Newfoundland examples. *American Journal of Science* 273, 594-621.
- 713
- 714 Authors' addresses: *Dr. Inna Yu. Badanina, Dr. Kreshimir N. Malitch* (*corresponding author), Department of
715 Geochemistry and Ore-Forming Processes, A.N. Zavaritsky Institute of Geology and Geochemistry, the Uralian
716 Branch of Russian Academy of Sciences, Pochtovy per. 7, Ekaterinburg, 620075; *Dr. Richard A. Lord*,
717 Department of Civil and Environmental Engineering, University of Strathclyde, Glasgow G4 0NG, United
718 Kingdom (richard.lord@strath.ac.uk); *Dr. Elena Belousova*, ARC Centre of Excellence for Core to Crust Fluid
719 Systems/GEMOC Key Centre, Department of Earth and Planetary Sciences, Macquarie University, Sydney,
720 NSW 2109, Australia (elena.belousova@mq.edu.au); Prof. Thomas C. Meisel, Department of General and
721 Analytical Chemistry, University of Leoben, Leoben 8700, Austria (thomas.meisel@unileoben.ac.at)
- 722

723 **Figure captions** for MS “Closed system behaviour of the Re-Os isotope system” by Badanina et
724 al.

725

726 **Fig. 1.** Simplified geological map of the Isles of Unst and Fetlar, showing major lithological units of the
727 Shetland Ophiolite Complex (after Flinn, 1996; 2001) and location of major PGE-rich chromitite sites at Cliff,
728 Harold’s Grave, North of Baltasound (NSB) and Hagdale including sample RL009 at Harold’s Grave area. The
729 trace of petrological Moho (PM) is also highlighted as are the harzburgites of the upper and lower nappes (UN
730 and LN, respectively). Grid lines are those of the UK National Grid (HP).

731 **Fig. 2.** Geological map of the best-preserved example of the ophiolite strathigraphy in the SOC, showing the
732 relationship of the chromitite quarries at Harold’s Grave (red arrow) to dunite pods in the mantle sequence and
733 the major chromitite occurrences North of Baltasound and Hagdale near or above the petrological Moho (after
734 Lord, 1991).

735 **Fig. 3.** Massive texture of chromitite sample RL009 cut for mineralogical and isotopic analysis.

736 **Fig. 4.** Chondrite-normalised PGE patterns of podiform (RL009) chromitite at Harold’s Grave (Shetland
737 ophiolite complex). Composition of chondrite according to McDonough and Sun (1995). Reference field of
738 podiform chromitites (in grey) after Melcher (2000).

739 **Fig. 5.** Back scattered electron images of euhedral composite PGM grains from podiform chromitite at Harold’s
740 Grave. LR - laurite; (Ir,Os) – Os-rich iridium; (Os,Ir) – Ir-rich osmium. Circles denote areas of laser ablation
741 MC-ICP-MS analyses; $^{187}\text{Os}/^{188}\text{Os}$ values correspond to those in Table 4. Scale bar is 30 microns.

742 **Fig. 6.** Back scattered electron images of secondary PGM assemblages in chromitite at Harold’s Grave. LR 1 –
743 laurite, LR 2 – Os-bearing laurite; Os – osmium; IRS - irarsite; PNLT – Ru-bearing pentlandite; CHR - chromite;
744 CHL – chlorite; numbers 1-7 denote areas of electron microprobe analyses corresponding to the same numbers
745 in Table 3. Circles denote areas of laser ablation MC-ICP-MS analyses.

746 **Fig. 7.** Composition of laurite (a and b) and Os-rich alloys (b) from podiform chromitite at Harold’s Grave in the
747 ternary diagrams Ru-Os-Ir, at. %. Symbols: *open circles*, laurite; *open squares*, Ir-rich osmium and *open*
748 *diamonds*, Os-rich iridium. In 7b, yellow area corresponds to miscibility gap between osmium and iridium
749 (Harris and Cabri, 1991).

750 **Fig. 8.** Histogram of Os isotope compositions of primary and secondary PGMs from chromitite at Harold’s
751 Grave.

752 **Fig. 9.** Models for the Re–Os evolution of the convecting mantle (modified after Shi et al., 2007). Horizontal
753 dark gray area corresponds to the osmium isotopic composition of PGM and chromitite from the Nurali massif.

754

755

756 **Tables** for MS “Closed-system behaviour of the Re-Os isotope system” by Badanina et al.

757

758 **Table 1.** Concentrations of PGE, Re (in ppb) and Os-isotopic composition of podiform chromitite
759 reported at Harold’s Grave

760 **Table 2.** PGM assemblages at the Harold’s Grave chromitite occurrence

761 **Table 3.** Selected electron microprobe (WDS) analyses of secondary PGMs from podiform chromitite
762 at Harold’s Grave

763 **Table 4.** Os isotope composition and model T_{MA} and T_{RD} ages of PGMs from primary PGM
764 assemblage at Harold’s Grave

765 **Table 5.** Summary of Os-isotope data for primary and secondary PGM assemblages from ophiolite
766 complexes

767

768 **ESM Appendix 1.** Os isotope composition and model T_{MA} and T_{RD} ages of PGMs from secondary
769 PGM assemblage at Harold’s Grave

Figure 1
[Click here to download high resolution image](#)

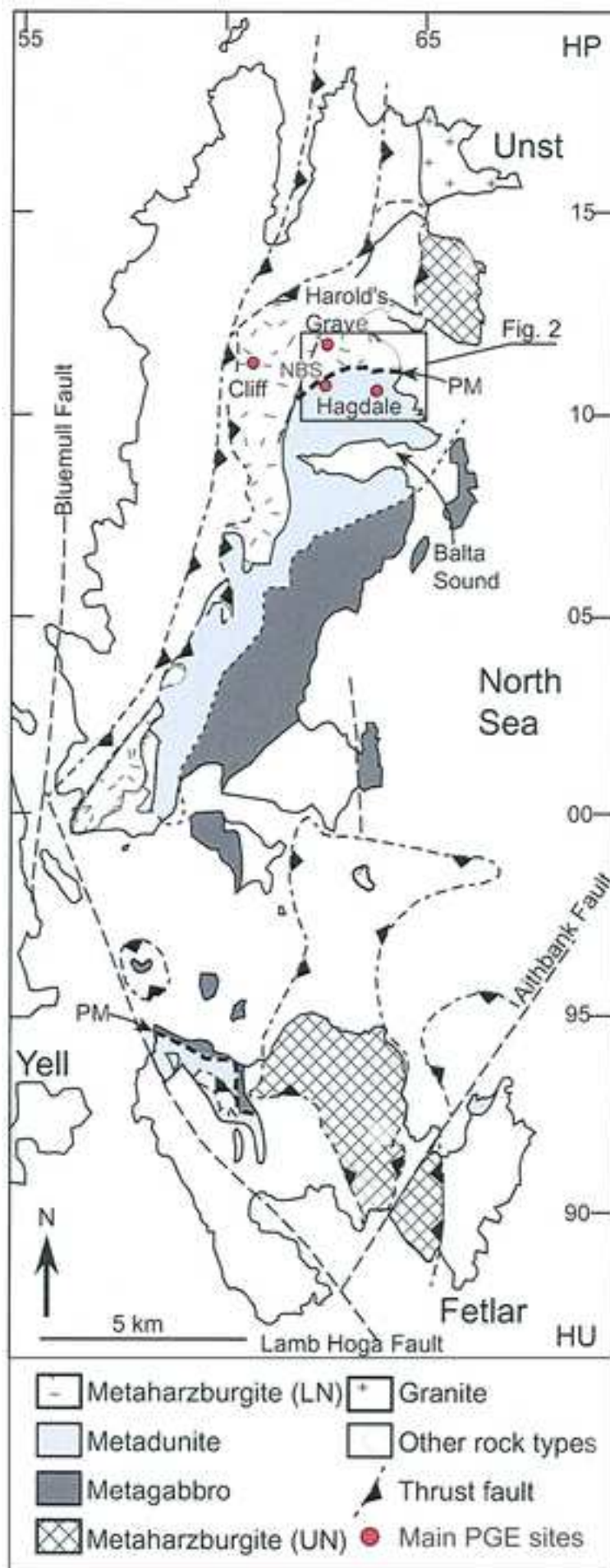


Figure 2
[Click here to download high resolution image](#)

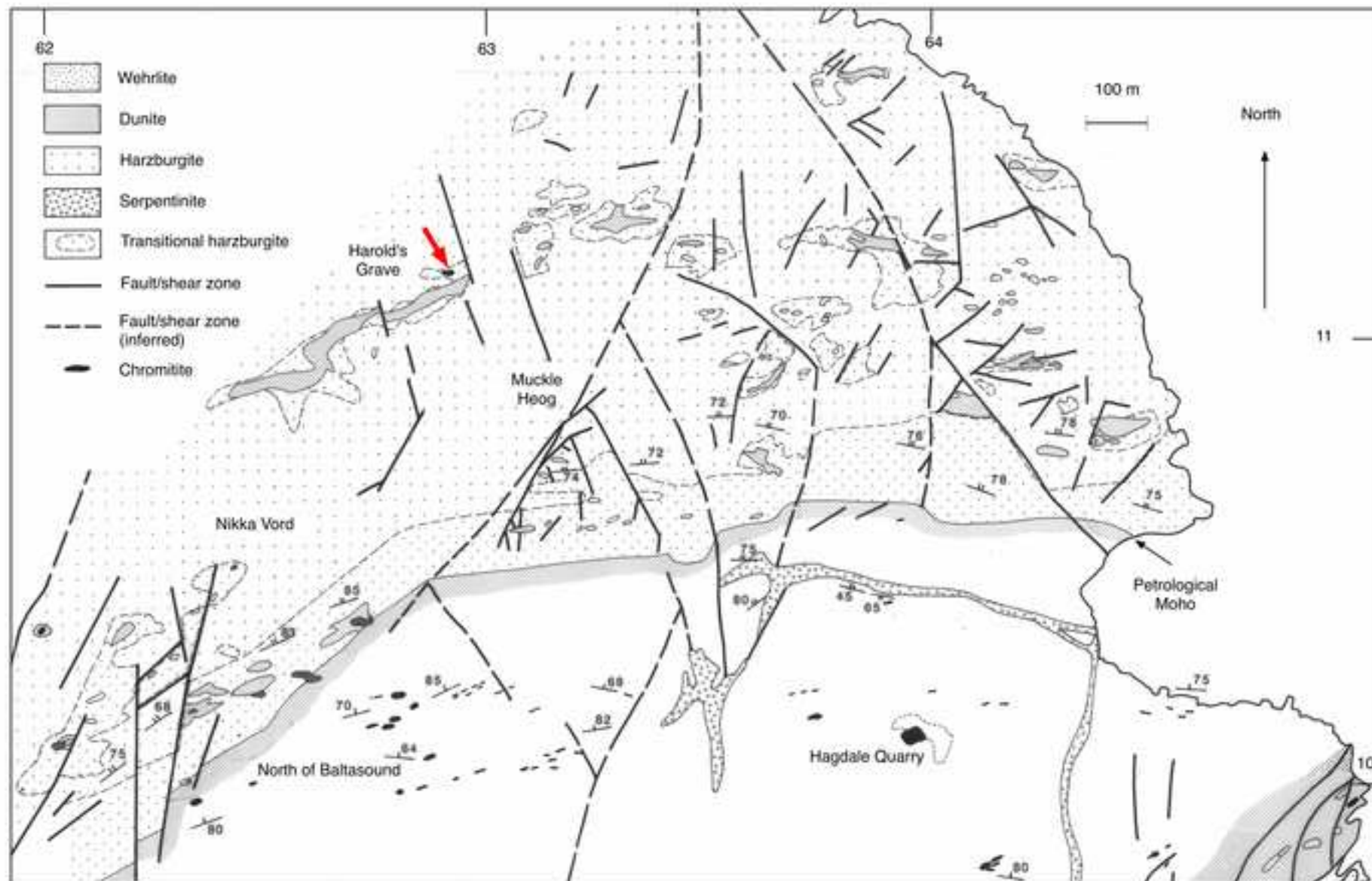


Figure 3
[Click here to download high resolution image](#)



Figure 4
[Click here to download high resolution image](#)

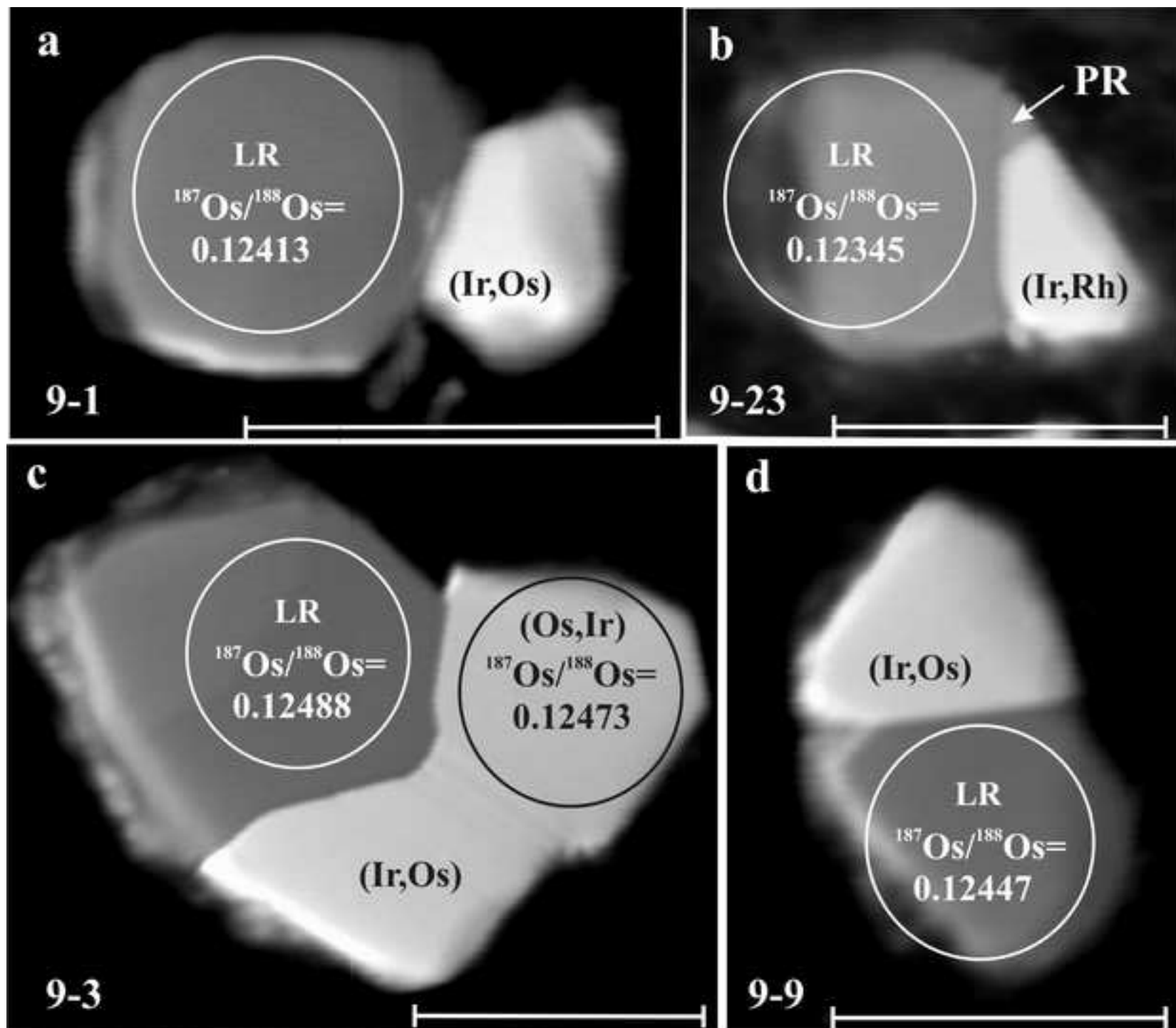


Figure 5
[Click here to download high resolution image](#)

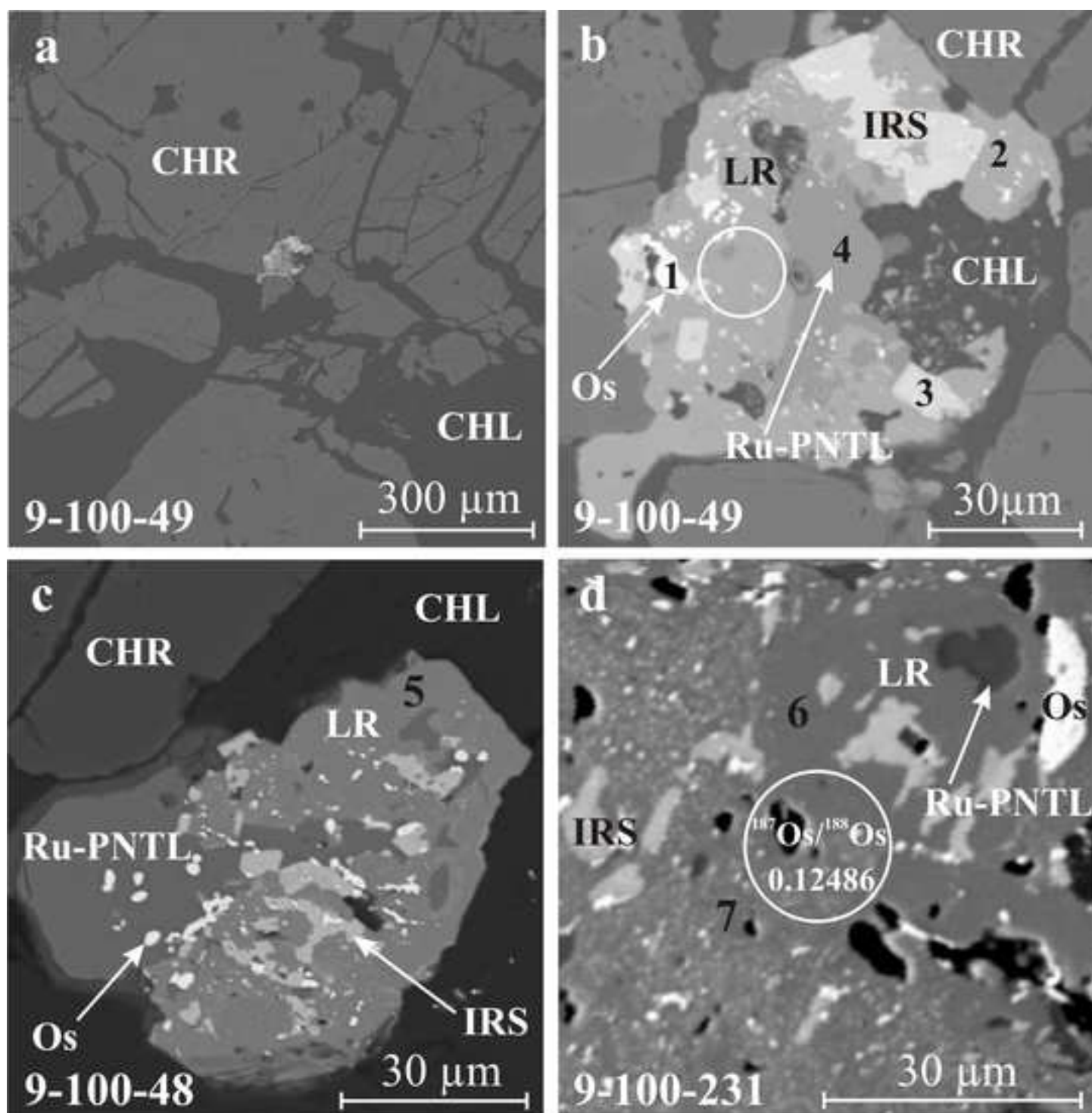


Figure 6
[Click here to download high resolution image](#)

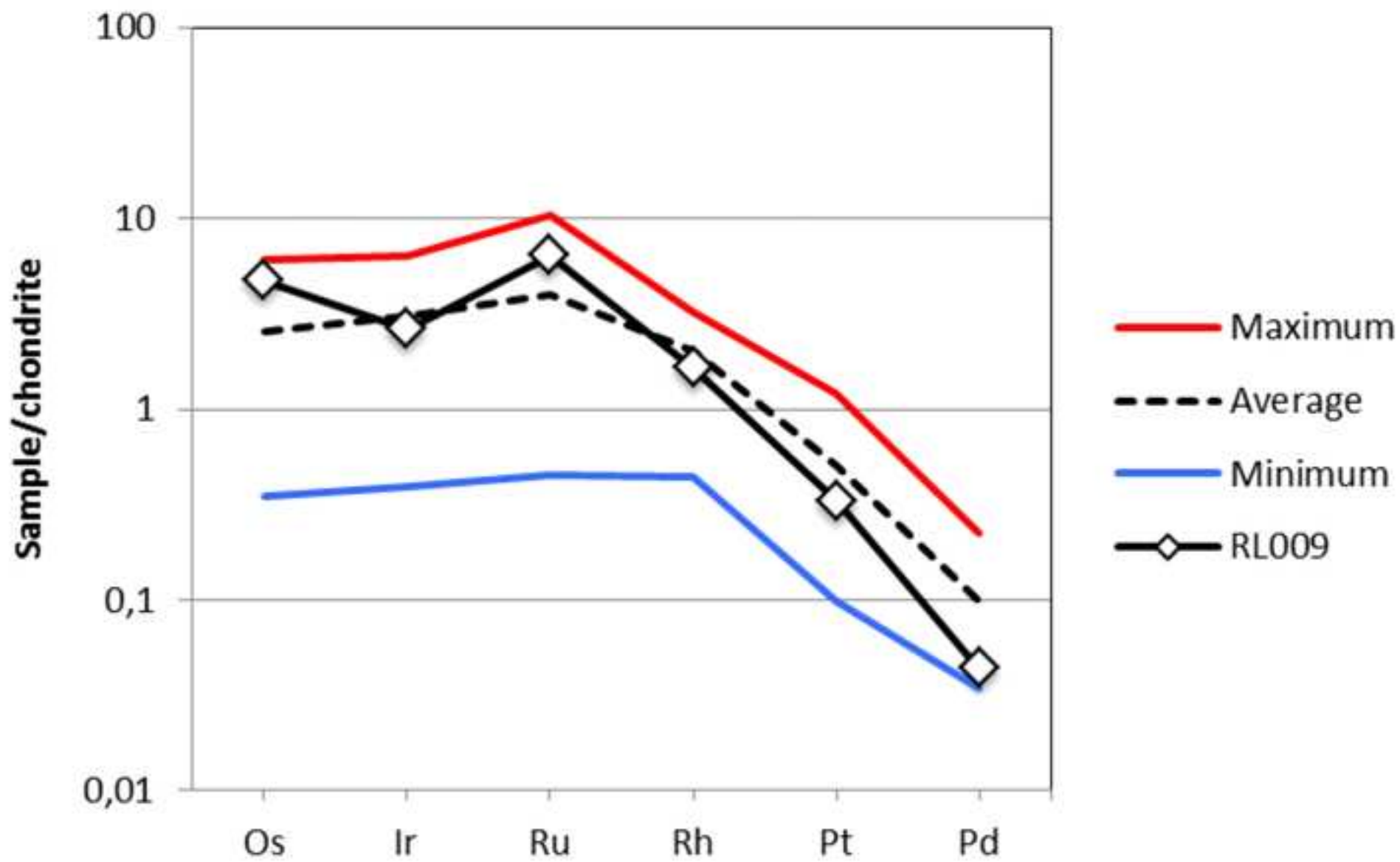


Figure 7
[Click here to download high resolution image](#)

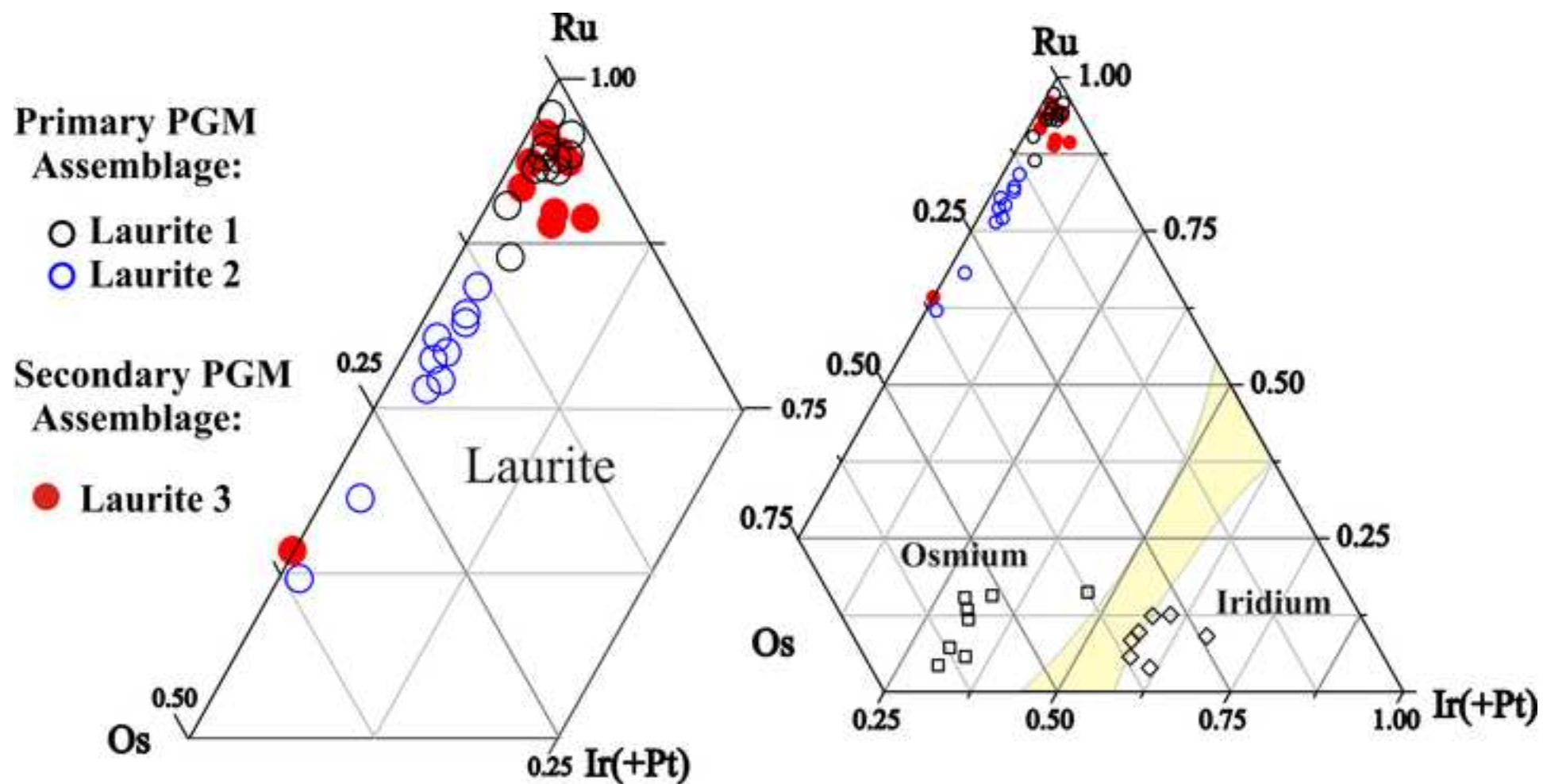


Figure 8
[Click here to download high resolution image](#)

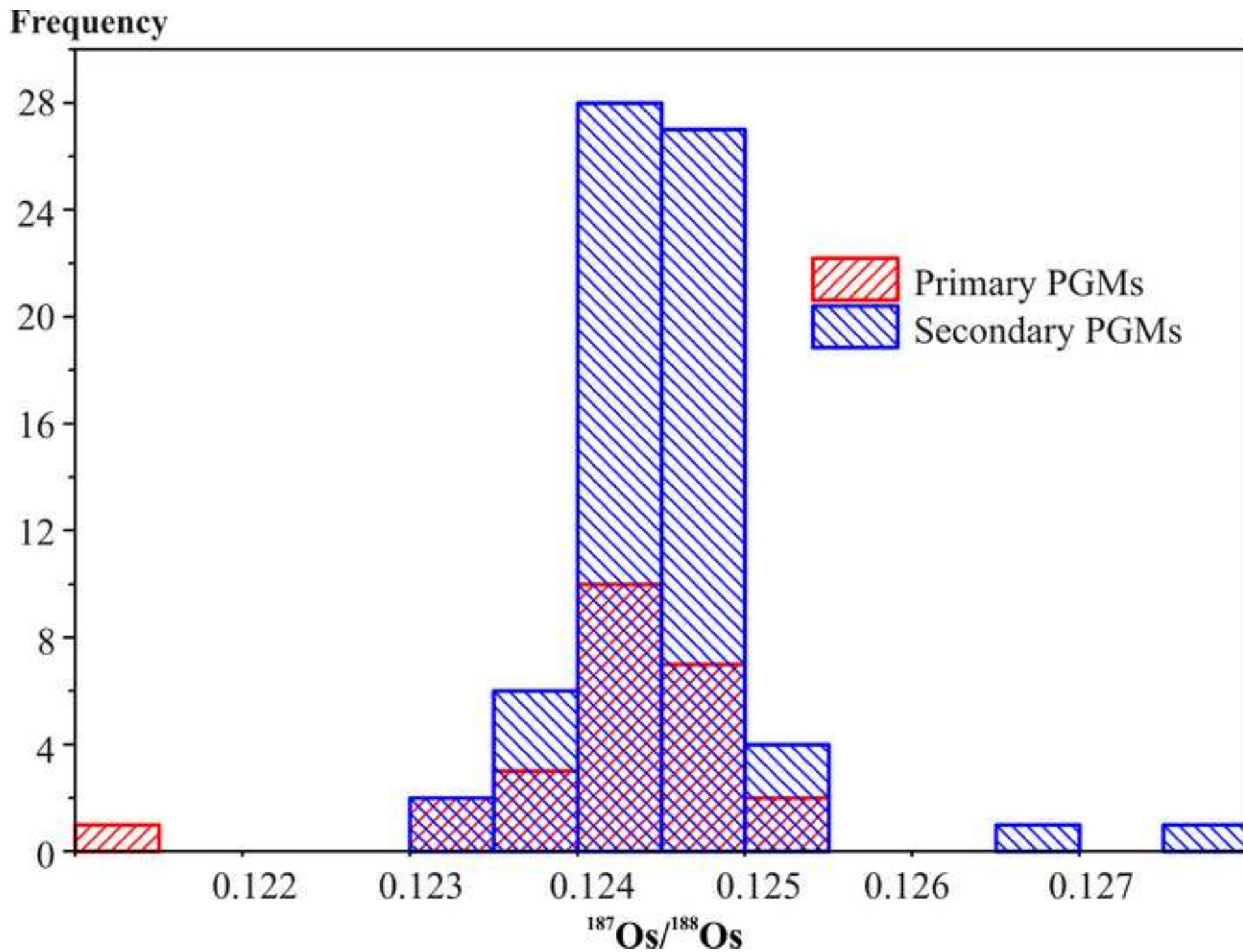


Figure 9
[Click here to download high resolution image](#)

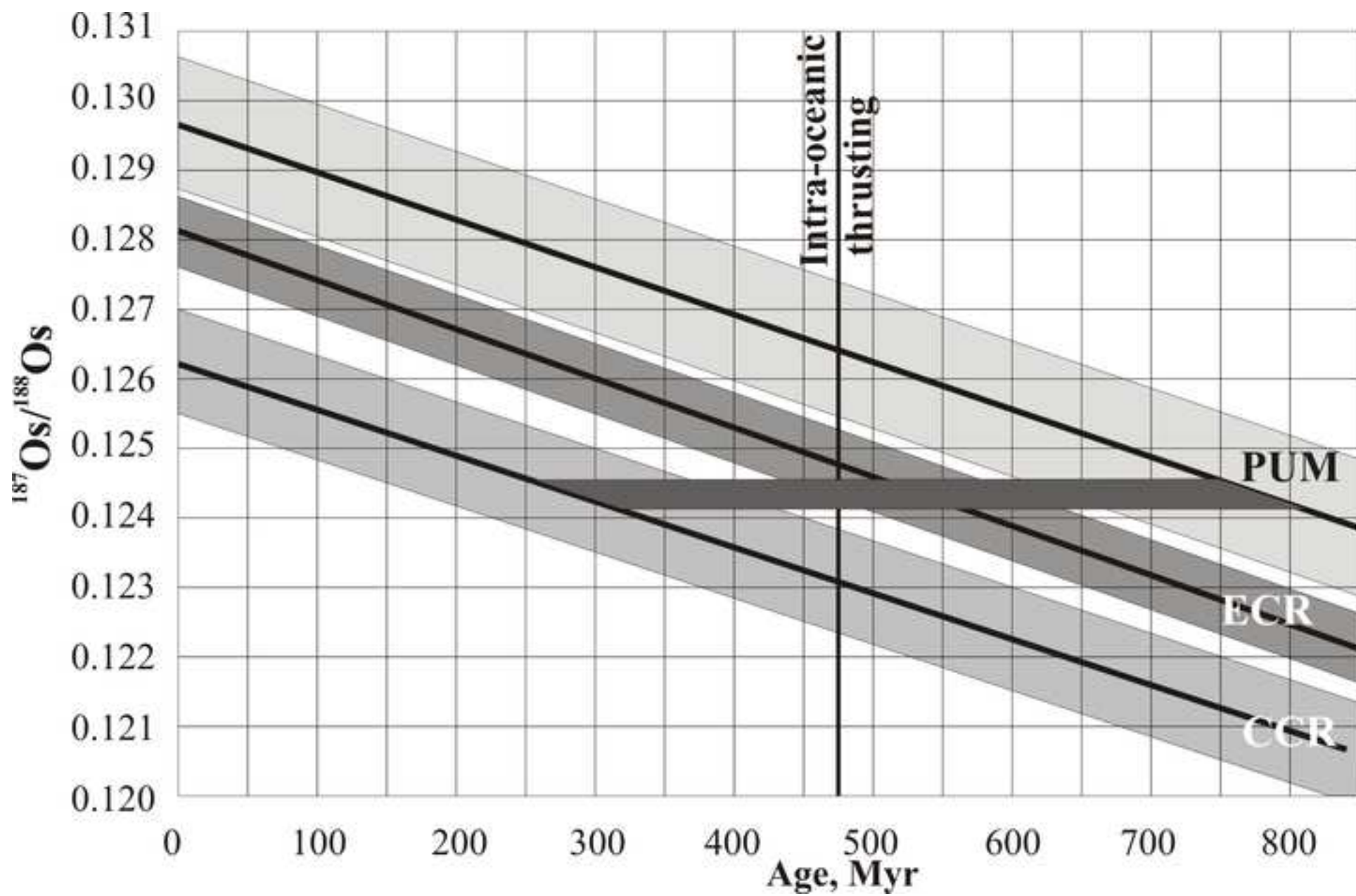


Table 1

Table 1. Concentrations of PGE, Au, Re (all in ppb) and Os-isotopic signature of chromitites from Harold's Grave

Sample ID	Lithology	Os	Ir	Ru	Rh	Pt	Pd	Au	Re	$^{187}\text{Os}/^{188}\text{Os} \pm 2\sigma$	ΣPGE	$\Sigma\text{IPGE}/\Sigma\text{PPGE}$	Source
Cr.	Chromitite	-	1803	4014	249	325	20	-	-	-	6411	9.79	Gunn et al., 1985
Cr.	Chromitite	-	831	740	129	250	19	-	-	-	1969	3.95	Gunn et al., 1985
F	Chromitite	800	1100	1800	220	370	3400	-	-	-	7690	0.93	Prichard et al., 1986
G	Chromitite	302	298	527	107	100	<8	-	-	-	1334	5.44	Prichard et al., 1986
RL069	Dunite host to RL070	170	180	320	57	170	24	<2	-	-	921	2.67	Lord, 1991
RL070	Chromitite layer	520	550	960	140	330	56	<2	-	-	2556	3.86	Lord, 1991
3	Chromitite	729	-	-	-	-	-	-	0.9237	$0.12523 \pm <0.000125$	-	-	Walker et al., 2002b
HG1	Chromitite	701	546	2356	-	459	112	-	0.0161	0.125542 ± 0.000042	4174	6.31	O'Driscoll et al., 2012
HG2	Chromitite	1693	1485	3440	-	1220	121	-	0.1223	0.124896 ± 0.000001	7959	4.94	O'Driscoll et al., 2012
HG2 Rep	Chromitite	997	667	3000	-	846	65	-	0.1168	0.125298 ± 0.000001	5575	5.12	O'Driscoll et al., 2012
HG3	Chromitite	1117	1012	2999	-	1124	122	-	0.0473	0.125229 ± 0.000006	6374	4.12	O'Driscoll et al., 2012
RL009	Chromitite	2302	1197	4517	214	333	24	-	-	-	8587	14.04	Badanina et al., 2013
HG11	Chromitite	2012	2127	3533	345	504	41	-	-	-	8562	8.62	Brough et al., 2015
HG5	Chromitite	1067	2073	2964	306	428	38	-	-	-	6876	7.91	Brough et al., 2015
HG7	Chromitite	1324	2270	3483	397	785	69	-	-	-	8328	5.66	Brough et al., 2015
HG1	Chromitite	1647	2040	3400	349	474	40	-	-	-	7950	8.21	Brough et al., 2015
HG1 rep	Chromitite	1587	1901	3252	331	431	42	-	-	-	7544	8.38	Brough et al., 2015
HG8	Chromitite	1479	2088	3183	344	685	36	-	-	-	7815	6.34	Brough et al., 2015
HG9	Chromitite	650	1159	2172	257	480	53	-	-	-	4771	5.04	Brough et al., 2015
HG4	Chromitite	1325	1974	3069	336	463	54	-	-	-	7221	7.47	Brough et al., 2015
HG6	Chromitite	2968	2861	7311	422	566	40	-	-	-	14168	12.78	Brough et al. 2015
RL009	Chromitite	2302	1197	4517	214	333	24	-	0.42	0.1240 ± 0.006	8587	14.04	Badanina et al. 2013, this study

Table 2. PGM assemblages at the Harold's Grave chromitite occurrence

	Primary assemblage (this study, Badanina et al., 2013)	Secondary assemblage (this study)	Additional minerals reported in other studies
Dominant Os-, Ir-, Ru-bearing, IPGE minerals and associations	Solitary grains of: Os-rich iridium (Ir,Os), or laurite (RuS ₂) Composite grains: mainly laurite + Os-rich iridium *, lesser laurite + Os-rich iridium* + Ir-rich osmium (Os,Ir)§ *with trace Rh and Pt §with trace Rh	Laurite, Os-rich laurite, Irarsite (IrAsS), Native osmium, Ru-pentlandite	
Rare phases, including Rh-Pt-Pd-bearing, IPGE minerals)	Ir-Rh alloy + Rh-rich sulfide (prassoite?) as composite grains with laurite)	Irarsite-hollingworthite ss series (IrAsS-RhAsS), Tolovkite (IrSbS), Geversite (PtSb ₂), Ru-rich oxide	Genkinite ((Pt,Pd) ₄ Sb ₃) ¹ , hongshiite (PtCu) ¹ , Pt-Pd-Cu alloy ¹ , mertieite I/II or stibiopaladinite ((Pd,Cu) ₅₋₁₁ (Sb,As) ₂₋₄) ¹ , Rh, Sb, S ¹ Rh, Ni, Sb ¹
Texture (shape)	Euhedral, regular internal phase boundaries	Subhedral to anhedral, complex, irregular, intimately intergrown	
Texture (position)	Inclusions enclosed by chromite	In chlorite or serpentine, in cracks within or interstitially to chromite	
Size µm	< 55 µm	< 500 µm	Laurite up to < 400 µm
Number of grains	156	904	

¹ Prichard and Tarkian, 1988² Prichard et al., 1994

Table 3. Selected electron microprobe (WDS) analyses of minerals from secondary PGM assemblage at Harold's Grave

Analysis	1	2	3	4	5	6	7
Sample	9-100-49	9-100-49	9-100-49	9-100-49	9-100-48	9-100-231	9-100-231
Figure	5b	5b	5b	5b	5c	5d	5d
Mineral	Osmium	Laurite	Irarsite	Ru-PNTL	Laurite	Laurite	Laurite
	wt. %						
S	0.00	37.05	11.36	30.41	38.26	37.89	36.59
As	0.00	0.00	26.11	0.00	0.00	0.00	0.00
Sb	0.00	0.00	0.00	0.00	0.00	0.00	0.00
Fe	0.00	0.00	0.00	21.82	0.00	0.00	0.00
Ni	0.00	0.00	0.00	34.63	0.00	0.00	0.00
Cu	0.00	0.00	0.00	0.00	0.00	0.00	0.00
Ru	0.87	53.56	3.14	12.22	57.28	56.23	52.42
Rh	0.00	0.00	4.54	0.00	0.00	0.00	0.00
Os	93.19	7.02	3.32	0.00	3.08	2.86	5.61
Ir	5.90	1.78	51.58	0.00	1.35	3.23	5.14
Pt	0.00	0.00	0.00	0.00	0.00	0.00	0.00
Total	99.96	99.41	100.05	99.08	99.97	100.21	99.76
	at. %						
S	0.00	66.73	33.31	46.27	66.92	66.77	66.50
As	0.00	0.00	32.76	0.00	0.00	0.00	0.00
Sb	0.00	0.00	0.00	0.00	0.00	0.00	0.00
Fe	0.00	0.00	0.00	19.06	0.00	0.00	0.00
Ni	0.00	0.00	0.00	28.78	0.00	0.00	0.00
Cu	0.00	0.00	0.00	0.00	0.00	0.00	0.00
Ru	1.63	30.60	2.92	5.90	31.78	31.43	30.22
Rh	0.00	0.00	4.15	0.00	0.00	0.00	0.00
Os	92.57	2.13	1.64	0.00	0.91	0.85	1.72
Ir	5.80	0.53	25.22	0.00	0.39	0.95	1.56
Pt	0.00	0.00	0.00	0.00	0.00	0.00	0.00
Ru number		93			97	97	95

Note. Analysis numbers refer to points on Fig. 5. Abbreviations: Ru-PNTL – Ru-bearing pentlandite; Ru number of laurite equals to $100 \cdot \text{Ru}_{\text{at.}\%} / (\text{Ru} + \text{Os})_{\text{at.}\%}$.

Table 4

Table 4. Os isotope composition, model T_{MA} and T_{RD} ages of platinum-group minerals from primary PGM assemblage at Harold's Grave

Sample, Figure	PGM assemblage	^{188}Os	$^{187}\text{Os}/^{188}\text{Os}$	Uncertainty (1σ)	$^{187}\text{Re}/^{188}\text{Os}$	$^{187}\text{Os}/^{188}\text{Os}(i)$	γOs	T_{MA} (Ga)	1σ (Ga)	T_{RD} (Ga)	1σ (Ga)
9-1_Fig. 4a	LR + (Ir,Os)	0.28	0.12402	0.00009	0.0001	<i>0.1240</i>	-3.19	0.579	0.013	0.579	0.013
9-2	LR + (Ir,Os)	0.25	0.12413	0.00007	0.0001	<i>0.1241</i>	-3.10	0.564	0.010	0.563	0.010
9-3-1_Fig. 4c	LR + (Os,Ir) + (Ir,Os)	0.29	0.12498	0.00006	0.0001	<i>0.1250</i>	-2.44	0.443	0.008	0.443	0.008
9-3-2_Fig. 4c	LR + (Os,Ir) + (Ir,Os)	0.22	0.12473	0.00009	0.0002	<i>0.1247</i>	-2.63	0.479	0.013	0.479	0.013
9-9_Fig. 4d	LR + (Ir,Os)	0.25	0.12447	0.00006	0.0001	<i>0.1245</i>	-2.83	0.515	0.008	0.515	0.008
9-15	LR	0.34	0.12508	0.00009	0.0001	<i>0.1251</i>	-2.36	0.429	0.013	0.429	0.013
9-19	Os-LR	0.23	0.12137	0.00007	0.0002	<i>0.1214</i>	-5.25	0.952	0.010	0.952	0.010
9-20	LR	0.12	0.12447	0.00009	0.0001	<i>0.1245</i>	-2.83	0.515	0.013	0.515	0.013
9-23_Fig. 4b	LR + (Ir,Os) + PR	0.09	0.12344	0.00011	0.0001	<i>0.1234</i>	-3.64	0.661	0.016	0.661	0.016
9-28	LR + (Ir,Os)	0.42	0.12520	0.00004	0.0001	<i>0.1252</i>	-2.26	0.412	0.006	0.412	0.006
9-29-1	LR + (Ir,Os)	0.18	0.12325	0.00016	0.0001	<i>0.1233</i>	-3.79	0.688	0.023	0.687	0.023
9-29-2	LR	0.23	0.12363	0.00009	0.0003	<i>0.1236</i>	-3.49	0.634	0.013	0.634	0.013
9-161	(Os,Ir) + (Ir,Os)	0.07	0.12407	0.00033	0.0003	<i>0.1241</i>	-3.15	0.572	0.047	0.572	0.047
9-146	LR + (Ir,Os)	0.44	0.12433	0.00005	0.0002	<i>0.1243</i>	-2.94	0.535	0.007	0.535	0.007
9-134	LR	0.23	0.12449	0.00007	0.0002	<i>0.1245</i>	-2.82	0.513	0.010	0.512	0.010
9-133	(Ir,Os,Ru)	0.15	0.12354	0.00015	0.0005	<i>0.1235</i>	-3.56	0.647	0.021	0.647	0.021
9-102	LR	0.86	0.12464	0.00003	0.0004	<i>0.1246</i>	-2.70	0.492	0.004	0.491	0.004
9-101	LR	0.46	0.12475	0.00005	0.0001	<i>0.1248</i>	-2.62	0.476	0.007	0.476	0.007
9-78	LR	0.13	0.12391	0.00009	0.0002	<i>0.1239</i>	-3.27	0.595	0.013	0.594	0.013
9-76	(Ir,Os)	0.33	0.12459	0.00010	0.0004	<i>0.1246</i>	-2.74	0.499	0.014	0.498	0.014
9-61	(Ir,Os)	0.12	0.12425	0.00009	0.0004	<i>0.1243</i>	-3.01	0.547	0.013	0.546	0.013
9-38	LR + (Ir,Os)	0.14	0.12491	0.00008	0.0001	<i>0.1249</i>	-2.49	0.453	0.011	0.453	0.011
9-37	LR + (Ir,Os)	0.30	0.12479	0.00006	0.0001	<i>0.1248</i>	-2.58	0.470	0.008	0.470	0.008
9-36	LR	0.44	0.12415	0.00010	0.0006	<i>0.1242</i>	-3.08	0.561	0.014	0.561	0.014
9-35	LR	0.28	0.12441	0.00007	0.0004	<i>0.1244</i>	-2.88	0.524	0.010	0.524	0.010
Average (n=25)						<i>0.1242</i>			0.550		0.550

LR – laurite, Os-LR – Os-bearing laurite, (Os,Ir) – osmium, (Ir,Os) and (Ir,Os,Ru) – iridium, PR – prassoite, T_{MA} and T_{RD} ages were calculated with ECR values estimated by Walker et al. (2002a) and a decay constant of $\lambda=1.666 \cdot 10^{-11} \text{ year}^{-1}$ (Smoliar et al., 1996). Uncertainties on model ages are based on within run errors only.

Table 5

Table 5. Summary of Os-isotope data for primary and secondary PGM assemblages from ophiolite complexes

Massif	PGM assemblage	$^{187}\text{Os}/^{188}\text{Os}$				$^{187}\text{Re}/^{188}\text{Os}$				$T_{\text{MA}}=T_{\text{RD}}$ (Ma)			
		Mean	Min	Max	Sd	Mean	Min	Max	Sd	Mean	Min	Max	Sd
Shetland	primary (n=25)	0.12422	0.12137	0.12520	0.00079	0.00022	0.0001	0.0006	0.00015	550	412	952	111
	secondary (n=69)	0.12452	0.12344	0.12763	0.00060	0.00028	0.0001	0.0024	0.00039	508	67	661	85
	primary and secondary (n=94)	0.12444	0.12137	0.12763	0.00066	0.00026	0.0001	0.0024	0.00034	519	67	952	94
Nurali*	primary (n=26)	0.12515	0.12486	0.12553	0.00020	0.00006	0.00001	0.00061	0.00012	420	365	461	29
	secondary (n=34)	0.12520	0.12474	0.12568	0.00022	0.00008	0.00001	0.00046	0.00011	412	344	478	32
	primary and secondary (n=60)	0.12518	0.12474	0.12568	0.00021	0.00007	0.00001	0.00061	0.00011	415	344	4780	31

Sd - standard deviation; * after Malitch et al. (2016)